Ferritic power plant steels: remanent life assessment and approach to equilibrium

H. K. D. H. Bhadeshia, A. Strang, and D. J. Gooch

The steels used in the power generation industry are almost always given a severe tempering heat treatment before they enter service. This might be expected to give them a highly stable microstructure which is close to equilibrium. In fact, they undergo many changes over long periods of time. This paper is a review of some of the methods which exploit the changes in order to estimate the life that remains in alloys which are only partly exhausted. IMR/308

Dr Bhadeshia is in the Department of Materials Science and Metallurgy, University of Cambridge, Cambridge CB2 3QZ, UK, Dr Strang is with Alstom Energy Ltd, Steam Turbines, Rugby CV21 2NH, UK, and Dr Gooch is with National Power plc, Windmill Hill Business Park, Swindon SN5 6PB, UK.

Introduction

Many of the safety critical components in power plant are made of steels developed to resist deformation when used in the range 450–600°C and 15–100 MPa.[1,2] Many of these components are expected to serve reliably for a period of about 30 years,[3] and it is these which are the subject of this review.

Given the long life span, the typical tolerable creep strain rate may be about 3×10^{-11} s^{-1} (~2% elongation over the 30 years). The design stress must be set to be small enough to prevent creep rupture over the intended life of the plant. Other damage mechanisms which must also be considered include fatigue, thermal fatigue, creep–fatigue, progressive embrittlement, corrosion/oxidation and, where relevant, deterioration caused by hydrogen.

The steels are able to survive for such long periods because the operating temperature is only about half of the absolute melting temperature, making the migration of atoms very slow indeed. Figure 1 illustrates the typical distance (~10 nm) diffused by iron or substitutional solute atoms during 1 h at 500°C. The longevity of iron alloys in power plant relies on the fact that the diffusivities are incredibly small, Fig. 1. Notwithstanding this, slow but significant changes are expected over the long service life.

Another reason why the changes that are expected over the years must occur at a slow rate is that the steels are generally severely tempered before they enter service. This gives them a very stable microstructure. The stability can be discussed in terms of the free energy stored in the material, as illustrated in Table 1. The stored energy of the plain carbon steel (Fe–C–Mn) is described relative to the equilibrium state which is a mixture of ferrite, graphite, and cementite without any defects. The phases in cases 1 and 2 involve the equilibrium partitioning of all elements so as to minimise free energy. In cases 3–5 the substitutional solutes are configurationally frozen. Cases 6 and 7 are for a classical power plant alloy. It is seen that the reduction in stored energy when the microstructure changes from the M_2X to $M_{23}C_6$ microstructure is very small. This means that it will occur at a correspondingly slow rate.

Another consequence of the small diffusion coefficients is that the dominant creep mechanism is the climb of dislocations over obstacles with the help of thermal energy. The obstacles are mainly carbide particles which are dispersed throughout the microstructure.

Suppose that the microstructure and the operating conditions do not change during service. The accuracy with which component life might then be predicted would depend only on the quality of the experimental data. Uncertain data lead to more conservative design with larger safety factors. There are many different kinds of design criteria, but as an example, the design stress σ for boiler components where close dimensional control is not vital is given by[5,6]

$$\sigma = \frac{\sigma_r(t_r)}{1{\cdot}1 \times \text{safety factor}} \quad \ldots\ldots\ldots (1)$$

where $\sigma_r(t_r)$ is the stress required to rupture a specimen over a time period t_r, and the factor of 1·1 allows for material thinning during manufacture. It was the practice 40 years ago to design for $t_r = 10^5$ h but power plant design lives are more typically at $2{\cdot}5 \times 10^5$ h.

For turbine components where dimensional tolerance is crucial, the design stress is defined in terms of the creep strain, for example,

$$\sigma = \frac{\text{stress to give specified strain in } t_r \text{ h}}{\text{safety factor}} \quad (2)$$

Table 1 Stored energy as function of microstructure, defined relative to microstructure for which stored energy is arbitrarily set to zero*

Case		Stored energy, J mol^{-1}
	Phase mixture in Fe–0·2C–1·5Mn wt-% at 300 K	
1	Ferrite, graphite, and cementite	0
2	Ferrite and cementite	70
3	Paraequilibrium ferrite and paraequilibrium cementite	385
4	Bainite and paraequilibrium cementite	785
5	Martensite	1214
	Phase mixture in Fe–0·1C–2·2Cr–1Mo wt-% at 873 K	
6	Ferrite and paraequilibrium cementite → ferrite and $M_{23}C_6$ (e.g. after extensive service)	0
7	Ferrite and paraequilibrium cementite → ferrite and M_2X (e.g. when steel enters service)	63

*Bainite and martensite have higher stored energies relative to ferrite because of strain energy contributions and solute trapping. The term 'paraequilibrium' means that the phase has the same ratio of iron to substitutional solute atoms as the parent phase from which it formed.

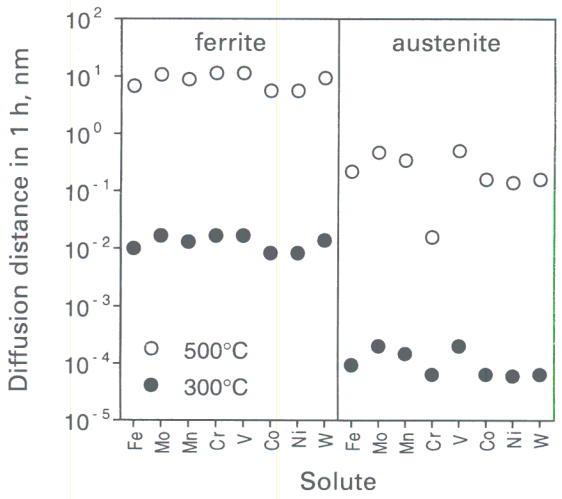

1 $2(Dt)^{1/2}$ estimate of distance diffused in 1 h, for iron and some substitutional solutes in iron, as function of temperature; D is diffusion constant and t time (after Ref. 4)

The specified strain may be in the range 0·1–0·5%. The safety factor is typically ~1·5 but can be reduced to ~1·3 if reliable long term data are available. Safety factors for assessment, as opposed to design, may be reduced if additional long term data become available.

The steels used are always heterogeneous and the service conditions vary over a range of scales and locations. The design life is therefore set conservatively to account for the fact that measured creep data follow a Gaussian distribution with a significant width. In spite of this, experience has shown to date that plant reaching its original design life generally has many further years of safe operating life remaining. To take advantage of this observation requires methods for the reliable estimation of the remaining life. The techniques used for this purpose are summarised in Table 2. Of the properties listed, no single measurement is sufficiently comprehensive to describe the steel with all requisite completeness. The implementation of a life extension procedure must consequently be based on broad considerations backed by more frequent inspections. Unfortunately, many inspection procedures can only be carried out on equipment which has been shut down.

Table 2 Some methods used in estimation of remaining life

Category	Property/test method
Mechanical	Hardness
	Tensile test
	Small specimen tests
	Impact toughness
	Component creep strain monitoring
Microstructural	Interparticle spacing
	Cavitation parameter
	Number density of cavities
	Volume fraction of cavities
	Area fraction of cavities
	Misorientation measurements
Other	Component temperature monitoring
	Ultrasonics
	Resistivity
	Density

Remanent life assessment is a very large subject. The focus of this paper is creep limited life, with only minor excursions into the important subjects of fatigue and embrittlement during service.[3] The components considered are those which might be expected to survive for many decades rather than components such as bolts which can be replaced relatively easily. The relative costs of replacement and life extension are also not addressed.

Critical regions for assessment

The first step in any assessment procedure is to check for the absence of any gross defects or embrittlement effects during service, which might limit safe operation before creep damage becomes important. Assuming that such defects are absent or can be repaired, regions are selected which are likely to be at the most advanced stages of deterioration. Components may be neglected in the assessment procedure if they are not life limiting. For example, failures of stub welds on steam headers are quite common but can be easily repaired.[5,6]

High and intermediate pressure rotors

The critical regions for the accumulation of damage in high temperature rotors are the bore (if one is present), the blade root fixings, balance holes, and stress concentrating features such as relief grooves, on the outer surface.[7]

In many rotors the position of maximum steady state strain accumulation is the rotor bore at the inlet stages. The potential failure mode which has to be guarded against is the initiation and growth of intergranular creep cracks to a size which could result in brittle fracture, either at cold startup due to centrifugal and thermal stresses or during overspeed. Ultrasonic and eddy current techniques are used to detect macroscopic defects but the direct examination of the bore surface for microscopic damage provides a significant challenge. It is however now possible to prepare and examine surfaces and also to remove samples for examination using remotely controlled devices.[8] A potential complication is that the region of maximum triaxial stress, which may be the area most susceptible to creep cavitation, is actually subsurface from the rotor bore. Some rotors are provided with bands or pips for the measurement of creep strain during service using datum measurements taken before service. Bore strains and remaining safe life can then be estimated through the use of critical strain data determined from experimental programmes.

Potential failure modes of blade root fixings[7] are either creep crack initiation and growth or shear failure due to excessive steady state creep strain accumulation. Axial entry root fixings can be examined directly or by the taking of plastic replicas without removing the blades but circumferential entry fixings are less accessible. Fortunately, the latter are generally less highly stressed. On some rotor designs the critical region is at the balance holes in the discs or at the transition between disc and body. These regions are more accessible for examination.

It is not often practicable to remove sufficient material from critical areas to produce specimens for direct determination of remaining life by accelerated creep testing. In this case samples may be prepared from 'cold' regions with the aim of positioning the original creep properties of the specific forging within the scatter band assumed by the design procedure.

High temperature headers

Steam headers (i.e. nodes where many large diameter, steam carrying pipes converge) are regarded as critical components because they are subject to large variations in temperature and pressure. They are also extremely expensive and difficult to replace.[5,6]

Boiler headers are built to many different designs. However, in general they involve butt and end cap welds between thick section pipes as well as branch and stub welds. Experience shows that creep damage generally occurs first in the vicinity of these weldments. Cracks may also be formed in the parent material ligaments between stub penetrations as a result of creep fatigue interactions generated by thermal stresses. In addition to these observed damage modes headers are accumulating microscopic or submicroscopic creep damage throughout operation which has to be assessed if the component is to be used beyond its original design life.

In general, steady state relaxed stresses are at a maximum at outer surfaces of cylindrical pressure vessels so that access is not a major problem. Direct observation, replication, and material sampling are then options for damage assessment by microstructural techniques. There are also techniques for removing samples for accelerated creep testing without compromising the integrity of the component.[9] However, the critical region is not always accessible. For example, (a) damage in welds generally initiates subsurface due to microstructural variations and (b) the position of maximum stress at stub penetrations is at the bore. In these cases stress analysis, service experience, and ultrasonic examination become the primary assessment tools.

Pipework

The areas most susceptible to creep damage in high pressure pipework systems are, as in headers, the welds. However, whereas in headers the stresses are generally determined by the pressure and thermal stresses alone, which are known or can be calculated, pipework systems are also subject to highly variable and largely unquantified external forces. This means that life management procedures for welds have remained largely experience based despite a great deal of effort expended in trying to devise quantitative prediction procedures.[10] Qualitative assessment of the severity of creep cavitation through examination of surface replicas is frequently used for pipe weld life management.

For operation beyond design life the condition of the parent material also has to be determined. Obtaining material for this is not a problem but the huge number of heats and individual forgings and castings in a typical system presents difficulties. Attention may then be concentrated on critical components within the system such as T-pieces and, in particular, bends. The latter are more highly stressed than straight pipes because of thinning and ovality produced during the bending process as well as the greater potential for stresses generated by system forces. Experience in continental Europe has confirmed the analytical prediction that outer surfaces are the most susceptible to creep damage but a key question is the profile of damage below the surface. However, this does not appear to always be the case; Viswanathan[11] has found subsurface cavitation to be the most severe. Methods which have been examined for quantification of the damage include the usual metallographic procedures as well as ultrasonic, magnetic, and resistivity based techniques. Surface replication techniques are obviously not appropriate when the damage is most severe within the bulk of the pipe.

Chests and casings

Valve chests and turbine casings are large complex components which are usually castings but sometimes closed die forgings. Internal cracking due to thermal fatigue is the most common mode of degradation encountered; procedures have been developed for this but are not within the scope of this review. There have been instances where poor design has led to creep damage in internal ligaments of valve chests but, in general, remanent life assessment of chests and casings has not been as great an issue as with the foregoing components. (The greater concern has been with the welds joining valve chests to pipework systems.)

Damage summation

A satisfactory way of representing creep damage C is to use a parameter ω which is normalised by its value at failure ω_r. The magnitude of ω_r will depend on the precise values of stress σ, temperature T, and any other variable which influences the creep process. Since these variables are not necessarily constant, the extent of damage is often written[12,13]

$$C = \sum_i \frac{\omega_i}{(\omega_r)_i} \quad \ldots\ldots\ldots\ldots\ldots\ldots\ldots\ldots\ldots\ldots \quad (3)$$

where ω is typically the time or the creep strain. Failure occurs when the sum achieves a value of unity. In practice, failure by creep or fatigue occurs in three stages: initiation of a crack, growth of the crack to a critical size and finally, much more rapid failure. The ultimate failure may be ductile if it occurs at high temperatures or brittle when it occurs at low temperature, for example during the startup or shutdown of plant.[11] The life fraction rule clearly does not distinguish between these stages, i.e. it does not embody mechanism. It should not be used for predictive purposes through a mechanism change.

Evans[12] argues that it is more appropriate to use the strain rather than the time, since the latter is not considered as a 'state variable'. In the context of thermodynamics, the state of a system can in principle be specified completely by a number of state variables (such as temperature, pressure) such that its properties do not depend at all on the path by which those

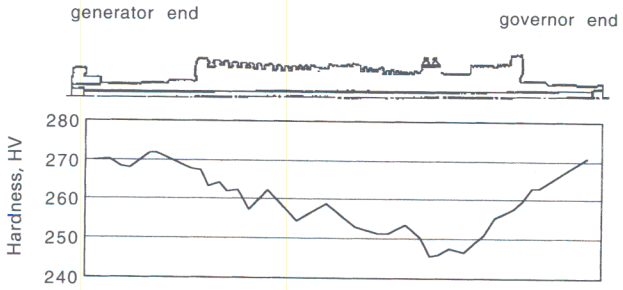

2 Hardness distribution on bore of 1Cr–Mo–V steel rotor after long term service. Note that steam entry point corresponds to location of minimum hardness. Corresponding hardness distribution in an unused rotor is more uniform with a variation of ±10 HV about mean (after Ref. 15)

variables were achieved. This clearly can not be the case even for the creep strain. This is because the extent of damage is expected to depend on the path by which a given value of strain is achieved, for example, whether the strain is localised at grain boundaries or uniformly distributed. This necessarily means that equation (3) is an approximation; as Evans states, it should be a reasonable approximation if the mechanism of creep does not change between the components of the summation. Thus, Cane and Townsend[14] conclude that the use of the life fraction rule in taking account of temperature variations is more justified than for variations in stress. This is because for the latter case, the dislocation networks become finer (relative to the carbide spacings) at large stresses. The network nodes then do not coincide with carbide particles, thus changing the mechanism of deformation. This is not the case with variations in temperature because the dislocation network then scales with the particle spacing. The failure of the life fraction rule is sometimes accommodated by empirically setting the limiting value of C to some positive value which is not unity.

Hardness

Figure 2 shows a hardness scan taken on the bore surface of a 1Cr–Mo–V HP–IP* rotor which had been in service for 174 000 h with an inlet steam temperature of 538°C. The hardness in the cold region near the generator is close to the value expected when the rotor entered service whereas there is a minimum in the region where the service conditions are expected to be most severe.

The hardness can in principle be used as an indicator for the state of the steel in its life cycle. Changes in hardness occur due to recovery, coarsening of carbide particles, and recrystallisation. All creep resistant power plant steels are severely tempered before they enter service. They are therefore beyond the state where secondary hardening is expected and the hardness can, during service, be expected to decrease monotonically. In these circumstances, an

*HP and IP stand for high pressure and intermediate pressure, respectively.

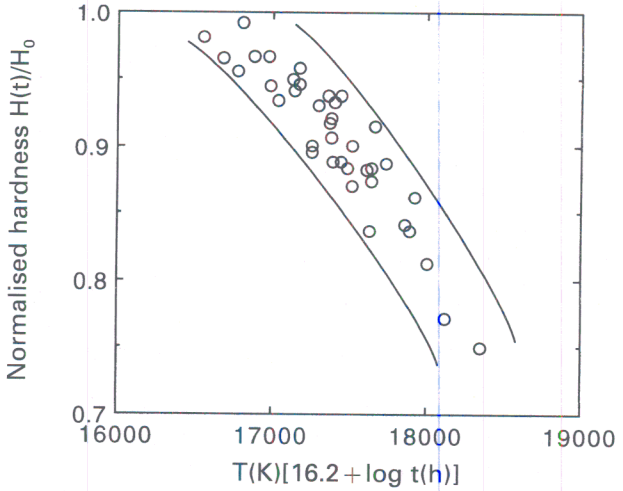

3 Change in normalised hardness as function of Larson–Miller parameter for 1Cr–Mo–V rotor steel (after Ref. 17)

Avrami equation adequately represents the changes in hardness

$$\xi = 1 - \exp(-k_A t^n) \quad \ldots\ldots\ldots\ldots \quad (4)$$

where t is the time, k_A and n rate constants, and ξ is given by

$$\xi(t) = \frac{H_0 - H(t)}{H_0 - H_\infty} \quad \ldots\ldots\ldots\ldots \quad (5)$$

where H_0 is the initial hardness, H_∞ hardness at the end of useful life, and $H(t)$ hardness at time t. The initial hardness may not be available when making life assessments, in which case an approximate value might be determined from the cold end of a rotor. Simpler linear relationships are used in practice. Thus, for 1Cr–Mo–V rotor steels, Gooch *et al.*[16] find

$$\frac{H(t,T)}{H_0} \approx 1{\cdot}605 \times 10^{-3} P - 4{\cdot}962 \times 10^{-8} P^2 - 11{\cdot}99$$

where

$$P = T(16{\cdot}2 + \log t)$$

with the temperature and time expressed in units of Kelvin and hours, respectively; P is the Larson–Miller parameter which helps rationalise time and temperature effects. The scatter and range of the data on which this equation is based are illustrated in Fig. 3.

Judging from data in the published literature for 1Cr–Mo–V steels, the hardness at the point where the microstructure is extensively annealed is likely to be around $H_\infty = 150$–190 HV for most power plant steels. Its main components include the intrinsic strength of iron and solid solution strengthening. The starting hardness is likely to be in the range $H_0 =$ 220–280 HV. Under power plant operating conditions, all that can be expected is a change in hardness of about 30–70 HV over a period of some 30 years. Thus, Roberts and Strang[18] have shown that the hardness can decrease by about 20% in the stressed regions of long term creep test specimens when compared with the unstressed parts. This is consistent with a ~25% reduction found by Maguire

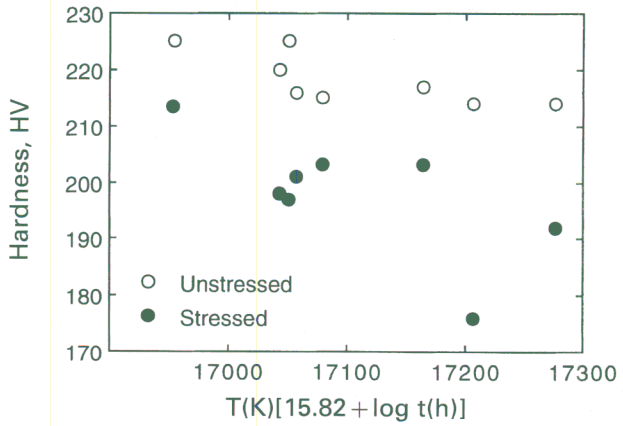

4 Changes in hardness of 1Cr–Mo–V steel during aging in temperature range 600–640°C. Samples were tempered at 700°C for 18 h before testing; effect of 700°C treatment is not included in calculation of time–temperature parameter plotted on horizontal axis; stress applied during each of tests was 93 MPa. Open circles are data from grips of creep test specimen, and solid circles represent measurements from gauge length. Data from Ref. 19

and Gooch.[19] Figure 4 shows the nature of the changes in hardness to be expected typically, as reported by Maguire and Gooch[19] for a 1Cr–Mo–V steel which was tempered at 700°C for 18 h before the aging at temperatures in the range 600–640°C.

Gooch and co-workers[16,17,19] have studied the hardness of a large number of 1Cr–Mo–V rotors. They find again that the reduction in hardness in the gauge length is always greater than that in the head of creep test samples

$$H(t)_{\text{gauge}} - H_0 = 1{\cdot}234[H(t)_{\text{head}} - H_0] - 14{\cdot}55 \quad \ldots\ldots\ldots (6)$$

where the subscripts 'gauge' and 'head' refer to the positions where the hardness tests were conducted. The observations indicate that gauge length softening is proportional to that in the head, apparently irrespective of the stress, temperature, or test duration. This is inconsistent with an empirical relationship used by Tack *et al.*[20]

$$\left.\begin{aligned}\frac{H(t) - H(t,\varepsilon)}{H(t) - H_\infty} &= b_1 + b_2 \ln \varepsilon \\ &\equiv b_2 \ln\left(\frac{\varepsilon}{\varepsilon_0}\right)\end{aligned}\right\} \quad \ldots\ldots (7)$$

where b_1, b_2, and ε_0 are empirical constants and ε is the strain. Unfortunately, values of these constants were not presented in the original paper. The equivalence that is expressed in equation (7) illustrates the fact that the equation can only be applied for strains greater than ε_0. For $\varepsilon < \varepsilon_0$ the equation predicts an increase in hardness which was not intended in the original representation. ε_0 can therefore be regarded as a threshold strain below which there is no effect of strain softening. If it is now assumed that ε_0 is large then the proportionality implied by Gooch *et al.*

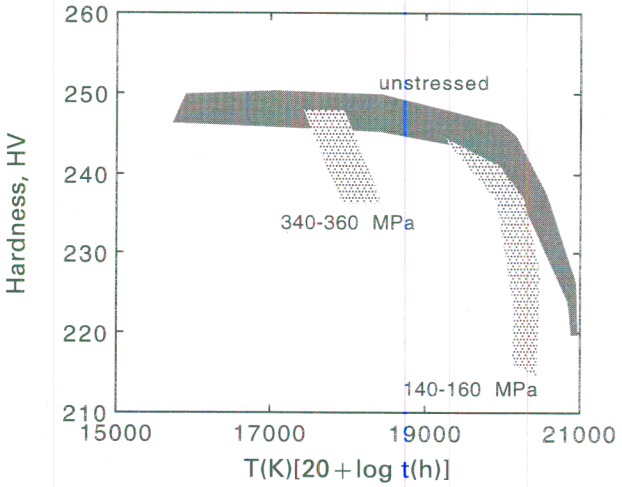

5 Hardness as function of Larson–Miller parameter and of stress for 1Cr–Mo–V rotor steel (after Ref. 15)

is recovered. Furthermore, the idea of a threshold strain seems to correlate with a threshold stress reported by Goto[15] and Strang *et al.*,[17] below which they did not observe any difference between the gauge and head regions.

Consistent with all the work described above, Goto[15] has also observed a greater rate of softening in strained regions, but with the difference relative to the unstrained regions being a strong function of the stress (Fig. 5). He therefore described the hardness in terms of an empirical relationship of the following form

$$\frac{H(t,T,\sigma)}{H_0} = 1 - b_{10}\sigma^{b_{11}}\frac{t}{t_r}\exp\left(-\frac{b_9}{T}\right) \quad \ldots (8)$$

where as usual, b_9, b_{10}, and b_{11} are empirical constants and t_r the time to rupture. On fitting these results to experimental data it was found that $b_{10} = 5500$, $b_{11} \approx 0$, and $b_9 = 8511$ K. This is a surprising result which suggests that the stress has no effect on the change in hardness, contradicting the data presented in Fig. 5. This anomaly arises because stress is implicitly included twice in equation (8). The rupture time t_r is a strong function of stress.

Given the variety of relationships proposed, it would be useful to reanalyse the entire collection of data either empirically or with a model that has some fundamental basis.

Goto has emphasised a quantitative relationship between the hardness and the rupture life, and hence the remaining life via the parameter t/t_r. Hardness is expected to be a crude indicator of remaining life. It does not, for example, relate easily to creep cavitation damage. Hardness tests are nevertheless useful in the regime of steady state creep before the onset of gross damage. This is evident from Fig. 5 where it is seen that specimens with the same hardness are at different life fractions.

There is a further complication, that the hardness of welded regions is likely to be inhomogeneous even when the welds are made with matching compositions. The potential location of failure is then difficult to

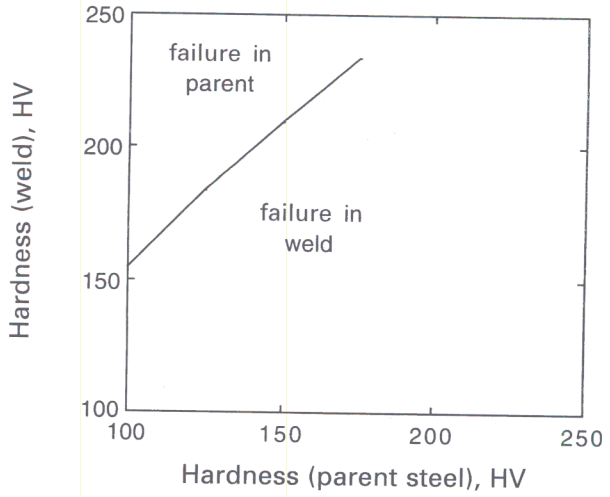

6 Data for 2·25Cr–1Mo steel and matching weld metal: curve represents locus of all points along which weld metal and parent metal have equal rupture lives. Note that for given life, weld must be harder than parent steel (after Ref. 20)

identify since creep ductility, creep strength, and creep strain may vary with position. The weld metal is likely to have a lower ductility than the parent material because of (a) the larger inclusion content, (b) the presence of regions of large grain size such as untransformed or partially transformed columnar grains or, (c) trace levels of creep embrittling species such as As, Sn, Sb, and P. It can not therefore be assumed that failure will always occur in the softest part of the joint. A harder weld may be needed to ensure the same rupture life as the parent steel (Fig. 6).

The heat affected zone of the parent material also has a highly inhomogeneous microstructure with the potential for narrow bands of either very large or very fine grains due to the different time–temperature history during welding. In general, a fine grain size leads to high ambient temperature hardness but low creep strength, though the latter may be compensated by high creep ductility. However, local variations in time–temperature history also result in extreme differences in carbide distribution. These may be the principal determinators of local hardness and creep strength though not necessarily ductility or rupture life.

Finally, the presence of (a) narrow bands of weak material in the heat affected zone and (b) the interface between weld metal and heat affected zone produces local regions of multi-axial stress. Increasing triaxiality reduces creep deformation rates but increases creep cavitation. The conflict between these two effects may result in either reduced or increased rupture life. Reduced ductility because of this effect is almost certainly a contributory factor in the so called 'Type IV' cracking in fine grained regions of low alloy ferritic weld heat affected zones. Conversely, the supporting effect of a strong parent material is the reason why it is often possible to specify a weld metal of lower creep strength if there is a concern over the ductility of a matching weld metal.

In short, the relationship between hardness and life of a weld is amazingly complex. Hardness may therefore be used only as a general indication of the state of the microstructure and only then if there are ample specific data for the materials and detailed welding processes concerned. This is well illustrated by the classic case of creep failures of low alloy ferritic welds, which may be in the weld metal or coarse or fine heat affected zones depending on chemical composition, weld process details, weld geometry or stress, or residual welding stress level.

Mechanism of strain softening

The observation that the hardness in the gauge length of the creep test specimen is smaller than that in the unstressed part is consistent with much basic work on the tempering of ferrite, bainite, and martensite. In this section the basic mechanisms by which strain softening might occur are reviewed. There are two kinds of studies, one in which the steel is deformed first and then tempered (strain tempering) and the other in which tempering occurs during creep deformation (creep tempering).

Strain tempering experiments involve the heat treatment of plastically deformed bainite or martensite. The process leads to large increases in strength with some loss in ductility and toughness. The strengthening that is obtained increases with the level of prior deformation but is not just a reflection of the effects of deformation on the microstructure. The subsequent tempering also causes a significant rise in strength by the precipitation of very fine alloy carbides on deformation induced defects.[21] This work emphasises that an increase in the dislocation density accelerates precipitation, probably by providing a larger number density of heterogeneous nucleation sites. The latter is well established for the control rolling of microalloyed steels, where the strain induced precipitation of carbonitrides on the dislocations introduced during the deformation of the steel is common.[22] Precipitation rarely occurs in the matrix in the absence of the dislocations.[23] There are many studies reviewed by Gladman,[22] which show that the acceleration of precipitation varies in proportion with the degree of deformation.[24–26]

It is established that the recovery and recrystallisation that occurs when bainite is tempered is accelerated during creep deformation.[27,28] Ridal and Quarrell[27] have also shown that in Mo containing bainitic steels, Mo_2C gives way more rapidly to the more stable M_6C carbide when the tempering occurs during creep deformation. The acceleration is greater for tests at lower temperatures, for higher creep strain rates, and for steels where the kinetics of the $Mo_2C \rightarrow M_{23}C_6$ reaction are slow in the absence of creep. The results are consistent with an enhancement of diffusion and nucleation rates, both of which can be attributed to the dislocations. Such effects are expected to be noticeable at low temperatures, high strain rates, and when the reaction rates are intrinsically slow. In the same work, Ridal and Quarrell also showed that the $M_7C_3 \rightarrow M_{23}C_6$ reaction during the tempering of Fe–C–Cr martensitic alloys is, if anything, slightly retarded by creep deformation. If this observation is certain then it implies that dislocations stabilise the M_7C_3. This effect is known for

other carbides in the context of martensite[29] and bainite,[30] where a large dislocation density retards the precipitation of ε-carbide by trapping carbon atoms at the dislocations. Whether this is applicable to the precipitation of alloy carbides remains to be demonstrated.

Interparticle spacing

Precipitates impede the motion of dislocations and any strength in excess of H_∞ is often related to the spacing λ between the particles (Cane and Williams)[31]

$$H - H_\infty \propto \frac{1}{\lambda} \propto t^{-1/3} \quad \ldots\ldots\ldots\ldots (9)$$

where it is assumed that $\lambda \propto t^{1/3}$ in order to be consistent with coarsening theory. There can be complications in this simple interpretation because there are generally two populations of particles, those on lath boundaries and other smaller precipitates in the matrix as well. The latter naturally tend to dissolve during any coarsening process.

Some results are illustrated in Fig. 7 for a 1Cr–0·5Mo steel.[32] The spacings are typically measured using transmission electron microscopy at a magnification of about ×20 000 with ~100 fields of view covering 30 μm^2 taken at random. The actual measurement involves counting the number of particles per unit area N_A and it is assumed that $\lambda = N_A^{-1/2}$. The amount of material examined in any transmission microscope experiment is incredibly small, so care has to be exercised in choosing representative samples of steel. In some cases, the microstructure may be inherently inhomogeneous. One example is the 12Cr and 9Cr type steels where there is a possibility of regions of δ-ferrite where the precipitation is quite different from the majority tempered martensite microstructure.

Obviously, hardness tests are much simpler to conduct when compared with the effort required to measure properly the particle spacings. A further complication is that there is frequently a mixture of many kinds of particles present, some of which continue precipitation during service whereas others dissolve. Thus, Battaini *et al.*[33] found that in a 12Cr–Mo–V steel, precipitation continues to such an extent during service that there is a monotonic decrease in λ. In fact, the distribution of particles was bimodal with peaks at 30 and 300 nm diameters. It is strange that they were only able to correlate the hardness against the changes in the coarser particles. For another steel (12Cr–Mo–V–W), Battaini *et al.* found an even more complex variation in the interparticle spacing with a maximum value in λ for the coarse particles.

It should be emphasised that the standard error in λ measurements is quite large, frequently larger than the variations observed. Given the difficulties of interpretation, and the experimental error, it is unlikely that λ measurements can be used as a satisfactory general measure of remaining life. The data can nevertheless be of use in the design of physically based creep models.

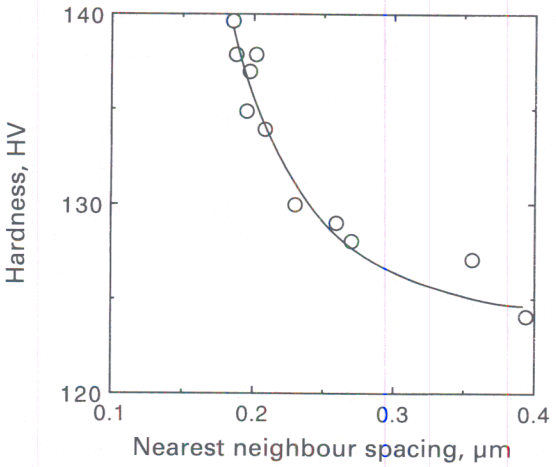

7 Hardness as function of nearest neighbour spacing of carbides in 1Cr–0·5Mo steel following creep tests at 630°C for variety of times (after Ref. 32)

Equilibrium phases

The simplest assumption in kinetic theory is to take a 'flux' to be proportional to the 'force', where the magnitude of the latter depends on the deviation from equilibrium. It follows that to understand the microstructural changes that happen in a steel during service, it is necessary first to consider the equilibrium state. Table 3 lists some of the common power plant alloys together with quotes from material specifications. It seems that the specifications are compiled by agreement between many vested interests and therefore tend to be unrealistically broad. Thus, many of the steels have only a maximum carbon concentration specified! The actual alloys are purchased by users to much tighter ranges than those given in Table 3.

The results of thermodynamic calculations which give the phase fractions and compositions as a function of the overall alloy composition and temperature, are given in Table 4 for the common power plant steels. The calculations have been done using the MTDATA computer program and SGTE (Scientific Group Thermodata Europe) database, taking into account the carbide phases and Laves phase listed.* The chemical elements considered are: carbon, silicon, manganese, chromium, nickel, molybdenum, vanadium, and niobium; nitrogen is not included but is known to be important in forming MX particles. Note also that some very careful work has recently identified an M_5C_2 in 1Cr–0·5Mo steels;[34] this phase has not been included in the analysis.

Changes in carbide chemical compositions

The cementite that forms in association with bainite or martensite has at first, a chemical composition which is far from its equilibrium composition. It therefore enriches with elements such as chromium

* The SGTE database contains assessed thermodynamic data which are interpreted by MTDATA to estimate phase diagrams, etc. MTDATA has been developed by the Thermochemistry Group of the National Physical Laboratory, Teddington, UK.

Table 3 Typical compositions (wt-%) of creep resistant steels used in power generation and petrochemical industries*

Designation	C	Si	Mn	Cr	Ni	Mo	V	Others
1Cr–0·5Mo	0·15	0·25	0·50	0·95	...	0·6	...	...
Range	0·08–0·18	0·10–0·35	0·40–1·00	0·70–1·10	...	0·40–0·60	...	...
0·5Cr–0·5Mo–0·25V	0·12	0·25	0·50	0·45	...	0·6	0·25	...
Range	0·10–0·15	0·10–0·35	0·40–0·70	0·30–0·60	<0·30	0·50–0·70	0·22–0·28	...
1Cr–Mo–V	0·25	0·25	0·75	1·10	0·70	1·00	0·35	...
Range	0·24–0·31	0·17–0·27	0·74–0·81	0·98–1·15	0·60–0·76	0·65–1·08	0·27–0·36	...
2·25Cr–1Mo	0·15	0·25	0·50	2·30	0·10	1·00	0·00	...
Range	<0·16	<0·5	0·3–0·6	2·0–2·5	...	0·9–1·1	...	...
Modified 2·25–1Mo	0·1	0·05	0·5	2·30	0·16	1·00	0·25	Ti 0·03; B 0·0024
3·0Cr–1·5Mo	0·1	0·2	1·0	3·0	0·1	1·5	0·1	...
Range	<0·16	<0·5	0·30–0·60	4·0–6·0	...	0·45–0·65	...	...
3·5N–Cr–Mo–V	0·24	0·01	0·20	1·70	3·50	0·45	0·10	...
Range	<0·29	<0·11	0·20–0·60	1·25–2·00	3·25–4·00	0·25–0·60	0·05–0·15	...
9Cr–1Mo	0·10	0·60	0·40	9·00	...	1·00	...	...
Range	<0·15	0·25–1·00	0·30–0·60	8·00–10·00	...	0·90–1·10	...	...
Modified 9Cr–1Mo	0·1	0·35	0·40	8·75	0·05	0·95	0·22	Nb 0·08; N 0·05
Range	0·08–0·12	0·20–0·50	0·30–0·60	8·00–9·50	<0·2	0·85–1·05	0·18–0·25	Nb 0·06–0·10; N 0·03–0·07; Al < 0·04
9Cr–0·5Mo–W–V	0·11	0·04	0·45	9·00	0·05	0·50	0·20	W 1·84; Nb 0·07; N 0·05
Range	0·06–0·13	<0·50	0·30–0·60	8·00–9·50	<0·40	0·30–0·60	0·15–0·25	Nb 0·03–0·10; N 0·03–0·09; Al < 0·04
12Cr–Mo–V	0·20	0·25	0·50	11·25	0·50	1·00	0·30	...
Range	0·17–0·23	<0·5	<1·00	10·00–12·50	0·30–0·80	0·80–1·20	0·25–0·35	...
12Cr–Mo–V–W	0·20	0·25	0·50	11·25	0·50	1·00	0·30	W 0·35
Range	0·17–0·23	<0·5	<1·00	10·00–12·50	0·30–0·80	0·80–1·20	0·25–0·35	W < 0·70
12Cr–Mo–V–Nb	0·15	0·20	0·80	11·50	0·75	0·55	0·28	Nb 0·30; N 0·06

*The range of compositions stated lie within the technical specification, but are really intended to reflect the variations observed in practice. The sulphur concentration is usually within the range 0·005–0·02 wt-%, and that of phosphorus within the range 0·005–0·025 wt-%.

during service in power plant, and might be used as a built-in recorder for the thermal energy felt by the steel.[31,35–43] The method has been used to estimate the effective service temperature of 0·5Cr–0·5Mo–0·25V steel to an accuracy of ±12 (Refs. 5, 6).

Virgin cementite

There is strong evidence to show that cementite and other iron based transition carbides grow by a para-equilibrium, displacive transformation mechanism when the precipitation is from martensite or bainite. This subject has been reviewed recently.[44] In this mechanism, the substitutional lattice is displaced into the new structure at a rate controlled by the diffusion of carbon to the transformation front. This is not terribly surprising given the very small distances over which the substitutional atoms can diffuse during the precipitation event (Fig. 1). Cementite, for example, precipitates in a matter of seconds during the tempering of martensite.

Of course, not all cementite in power plant steels comes from the bainite or martensite reactions. Many low alloy steels contain small quantities of pearlite. The cementite which is a constituent of pearlite grows by a reconstructive transformation mechanism in which all of the atoms diffuse in a way which minimises strain energy. But the diffusion at the same time allows species of atoms to partition into phases where they are most comfortable. Consequently, the cementite within pearlite always has a chemical composition which is closer to equilibrium. This is illustrated in Fig. 8*a*, where the cementite when it first forms, is seen to be richer in chromium for pearlite than for bainite. This is the case even when the pearlite and bainite grow at the same temperature.[45]

Naturally, the cementite will tend towards its equilibrium chemical composition when exposed to elevated temperatures for prolonged periods of time. This generally means that its substitutional solute content increases with time. It can be shown[39] that this change is given by

$$t = \frac{\pi[x^{\theta}(c^{\theta} - \bar{c})]^2}{16 D_{\alpha}(\bar{c} - c^{\alpha\theta})^2} \quad \ldots\ldots\ldots\ldots \quad (10)$$

Table 4 Mole fractions of precipitate phases in steels listed in Table 3, when at equilibrium at 565°C

Designation	M_2X	M_3C	M_7C_3	$M_{23}C_6$	M_6C	Laves	NbC	NbN	VN
0·25Cr–Mo–V	0·0053	...	...	0·0247	...	...	...	...	...
1Cr–Mo–V	0·0089	...	...	0·0412	...	...	...	...	...
2·25Cr–1Mo	...	...	...	0·0335	...	...	...	...	...
Modified 2·25Cr–1Mo	...	...	...	0·0211	0·0019	...	...	...	...
3·0Cr–1·5Mo	...	...	...	0·0185	0·0057	...	...	...	...
3·5Ni–Cr–Mo–V	0·0009	...	0·0161	0·0285	...	...	...	...	...
9Cr–1Mo	...	...	...	0·0222	...	...	...	...	...
Modified 9Cr–1Mo	...	...	...	0·0222	...	...	...	0·0009	0·0030
9Cr–0·5Mo–W–V	...	...	...	0·0248	...	0·0135	...	0·0008	0·0032
12Cr–Mo–V	...	...	...	0·0443	...	...	...	...	...
12Cr–Mo–V–W	...	...	...	0·0444	...	0·0007	...	...	...
12Cr–Mo–V–Nb	...	...	...	0·0318	...	...	0·0006	0·0029	0·0018

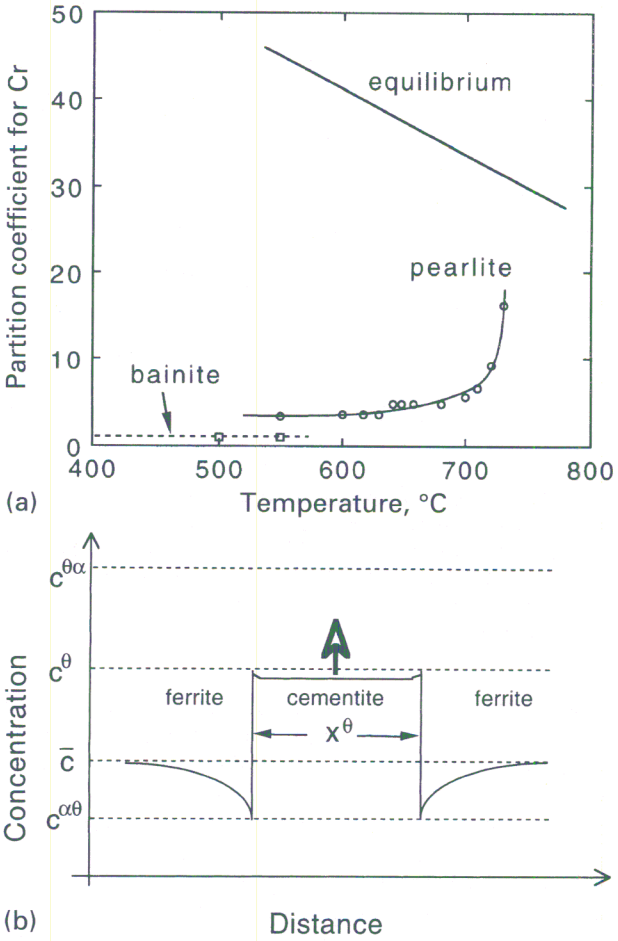

8 *a* partition coefficient for Cr in cementite, when cementite is part of bainite or pearlite, together with equilibrium data,[45] partition coefficient is ratio of concentration in cementite to that in ferrite, and *b* solute concentration profile that develops during enrichment of cementite particle

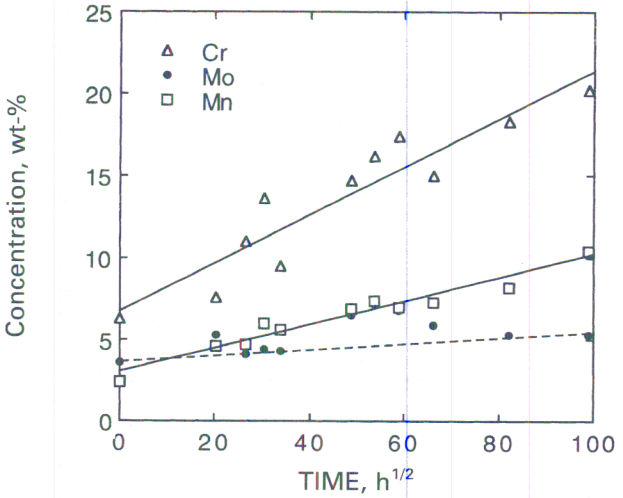

9 Measured changes in chemical composition of cementite particles as function of time$^{1/2}$ during aging at 550°C: steel composition Fe–0·1C–0·24Si–0·48Mn–0·84Cr–0·48Mo wt-%, heat treated to give fully bainitic microstructure, stress relieved at 730°C for 1 h and then tempered at 550°C for times illustrated, data from Ref. 38

where it is assumed that the particle is in the form of a thin plate of thickness x^{θ}, t the time at the annealing temperature, c^{θ} the average solute concentration in cementite (θ) at time t, D_{α} the diffusion coefficient of the substitutional solute in ferrite, $c^{\alpha\theta}$ the solute concentration in ferrite which is in equilibrium with that in cementite, and $\bar{c}$ the initial concentration of solute in the carbide (Fig. 8*b*). Note that c^{θ} is not the solute concentration $c^{\theta\alpha}$ in cementite which is in equilibrium with ferrite. The diffusion flux in the ferrite is so small that the solute concentration in the cementite at the boundary can not build up to the equilibrium level since any enrichment at the interface is relieved by diffusion within the cementite. This is because $(\bar{c} - c^{\alpha\theta})$ which drives the diffusion within the ferrite is much smaller than $(c^{\theta\alpha} - \bar{c})$, i.e. the solubility of elements such as chromium is much larger in cementite than in ferrite. It follows that in spite of the diffusion flows, the concentration distribution in the cementite is always likely to be quite uniform. This is a useful result since it makes it reasonable to determine the particle composition using microanalysis techniques which gather information from the entire particle. Thus the solute concentration in the cementite rises uniformly from $\bar{c}$ to $c^{\theta\alpha}$.

Equation (10) indicates that the change in composition $(c^{\theta} - \bar{c})$ should vary with $t^{1/2}$ during isothermal annealing; this is described as a parabolic law. This contrasts with the common assumption made even today, that the change should follow $t^{1/3}$ kinetics. It is often not possible in practice to distinguish between the two exponents; the experimental data give reasonable linear fits with either relationship. However, values of the diffusion coefficient extracted from such plots are only correct in the case for parabolic kinetics.[46] This confirms the physical significance of equation (10), which can be extrapolated with more confidence than the $t^{1/3}$ relationship. An additional advantage is that the effect of the steel chemistry is explicitly included in equation (10) via the equilibrium and average compositions, so that data from many different alloys can be interpreted together.

Figure 9 shows experimental measurements of the composition of cementite as a function of tempering time, for a microstructure which was initially fully bainitic.[47,48] The steel composition is Fe–0·1C–0·24Si–0·48Mn–0·84Cr–0·48Mo wt-%; the reason why the cementite composition is richer than the average is because a stress relief heat treatment was given before aging. There are a number of important features in this graph other than the fact that the parabolic law is verified. It is obvious that the largest changes are observed for chromium, which would therefore be a good element to monitor. This is because the solubility of Cr in the cementite is much larger than that of Mn or Mo (Table 5). Notice that the solubility varies with temperature, becoming smaller with increasing temperature.

It should also be emphasised that the equilibria listed in Table 5 are steel specific and will vary greatly within the range of power plant alloys used typically in industry. A simple method for estimating the values is to write the partition coefficient of alloying element

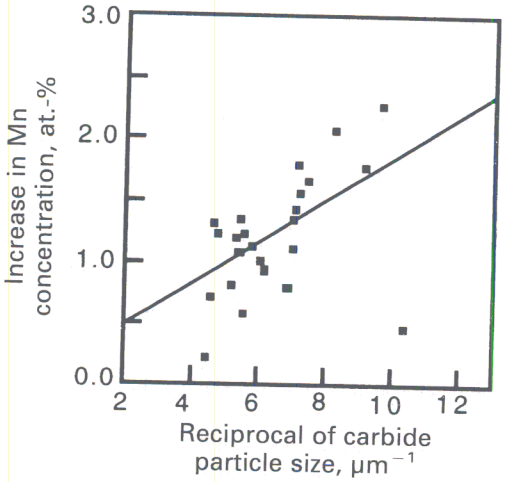

10 Size dependence of cementite enrichment; annealed at 565°C for 4 weeks[47,48]

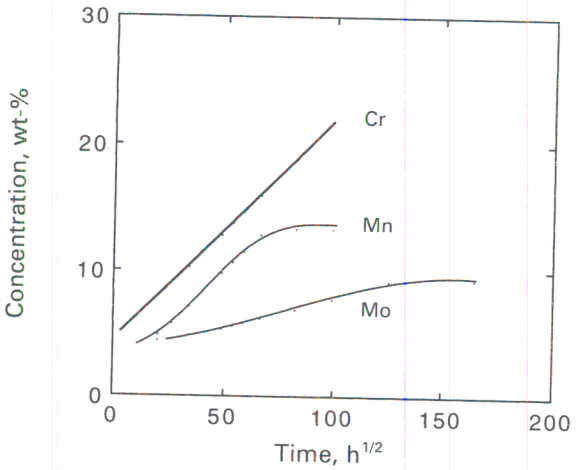

11 Calculated changes in chemical composition of cementite particles as function of time$^{1/2}$ during aging at 550°C: steel composition Fe–0·1C–0·24Si–0·48Mn–0·84Cr–0·48Mo wt-%: calculations made using finite difference method[39]

Z as follows

$$k_Z = \frac{c^{\theta\alpha}}{c^{\alpha\theta}} \approx \exp\left(\frac{A + BT}{RT}\right) \quad \ldots\ldots\ldots (11)$$

where the parameters A and B are listed in Table 6.[49] The partition coefficient only gives a ratio – to calculate the actual concentrations requires the following further relationship which derives from mass balance

$$\bar{c} = c^{\theta\alpha} V_\theta + \frac{c^{\theta\alpha}}{k_Z} - \frac{c^{\theta\alpha} V_\theta}{k_Z} \quad \ldots\ldots\ldots (12)$$

V_θ, the volume fraction of cementite in the alloy, can be estimated using the lever rule with carbon, so that the equilibrium compositions of the two phases can easily be calculated as a function of heat treatment and average composition.

Another feature highlighted by the parabolic law is the dependence of enrichment on the particle size x^θ. Smaller particles enrich faster and saturate earlier because they are smaller reservoirs for solute (Fig. 10).

The model described above predicts parabolic kinetics, which can be considered to have been verified by published experimental data. Although the data refer to time periods as long as 10 000 h, the time scales of interest are much larger, of the order of 250 000 h. Data can of course be obtained from steels which have been in service but they can be quite unreliable because the history is then uncertain. It would not be safe to extrapolate the parabolic law to very long times, because the analytical expression does not account for a phenomenon known as soft impingement. In this, the diffusion fields of adjacent particles begin to overlap and significantly interfere, slowing down the enrichment process until it stops completely when equilibrium is achieved. Such a process can not easily be treated analytically. Bhadeshia[39] has used a finite difference method instead; some results are presented in Fig. 11, for precisely the experiments reported by Afrouz *et al.*[38] The parabolic law is a good approximation during the early stages but the effect of soft impingement is to cause deviations with a complete halt when the carbide saturates with the solute concerned. Manganese and molybdenum do so quite rapidly for this particular example. Thus, the numerical method (finite difference) can be used to extrapolate to very long times.

Table 5 Calculated equilibrium concentrations for Fe–0·1C–0·24Si–0·48Mn–0·84Cr–0·48Mo wt-% alloy used by Afrouz *et al.*;[38] calculations are specific to this steel

	Equilibrium wt-%, 703°C		Equilibrium wt-%, 550°C	
Element	$c^{\alpha\theta}$	$c^{\theta\alpha}$	$c^{\alpha\theta}$	$c^{\theta\alpha}$
Cr	0·52	21·3	0·30	36·0
Mo	0·40	5·8	0·34	9·3
Mn	0·38	6·7	0·29	13·2

Pearlite

It has been emphasised that the substitutional solute/iron atom ratio is the same everywhere in a bainitic or martensitic microstructure as in the alloy as a whole. This is not the case for pearlite where the reconstructive mechanism of transformation ensures that the cementite is enriched with substitutional solutes, though often not to the extent expected from equilibrium. This makes it impossible to predict the initial composition of the cementite in pearlite. It turns out that for calculation purposes, this is not a serious problem for long aging times, since the degree of enrichment then tends to be much larger than the starting solute level (Fig. 12).

Table 6 Compilation of parameters used for calculation of partition coefficients[49]

Element Z	A, J mol^{-1}	B, J mol^{-1} K^{-1}
Cr	47 028	−17·45
Mn	42 844	−20·21
Mo	27 363	−5·86
Ni	−2619	−2·80
Si	0	−25·10

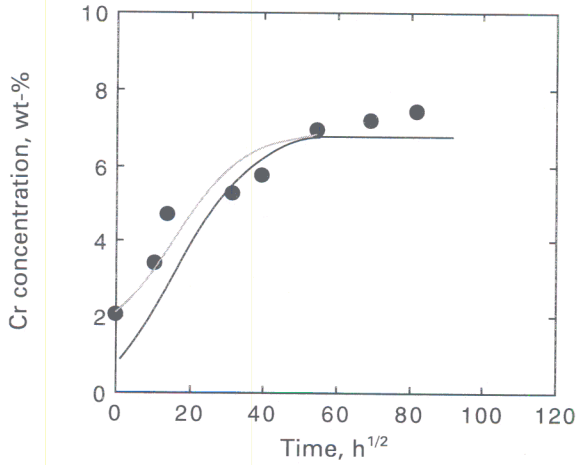

12 Data for enrichment of cementite associated with pearlite, and calculated curves assuming zero enrichment at $t=0$ (continuous curve) and finite enrichment at $t=0$ (broken line) (after Ref. 45)

Effect of carbon

There are two effects which depend on the carbon concentration of the steel. The ternary Fe–C–Cr phase diagram on the $(Fe,X)_3C/\alpha$ field shows that an increase in the carbon concentration is accompanied by a decrease in the equilibrium concentration of chromium in the carbide. Thus, the carbide enrichment rate is expected to decrease. A further effect is that the volume fraction of cementite increases, in general leading to an increase in particle thickness and volume fraction. The thickness increase retards the rate of enrichment (equation (10)). If the carbide particles are closer to each other then soft impingement occurs at an earlier stage, giving a slower enrichment rate at the later stages of annealing.

Local variations in carbon concentration may have a similar effect to changes in average concentration. Such variations can be present through solidification induced segregation, or because of microstructure variations caused by differences in cooling rates in thick sections. It is well known that the microstucture near the component surface can be fully bainitic with the core containing a large amount of allotriomorphic ferrite* in addition to bainite. In the latter case, the bainite which grows after the allotriomorphic ferrite, transforms from high carbon austenite. The associated carbides are then found to enrich at a slower rate (Fig. 13*a*). This discussion emphasises the role of carbon.

High alloy steels, alloy carbides

The vast majority of steels used in the power generation industry have a total alloy concentration less than 5 wt-%, but there are richer martensitic alloys such as the 9Cr–1Mo, 12Cr–1Mo–V destined for more stringent operating conditions. For low alloy steels, the initial carbide phase found immediately

* Ferrite which grows by a diffusional mechanism is termed allotriomorphic when its outward form does not reflect the symmetry of its crystal structure. It commonly nucleates and grows preferentially along the austenite grain surfaces.

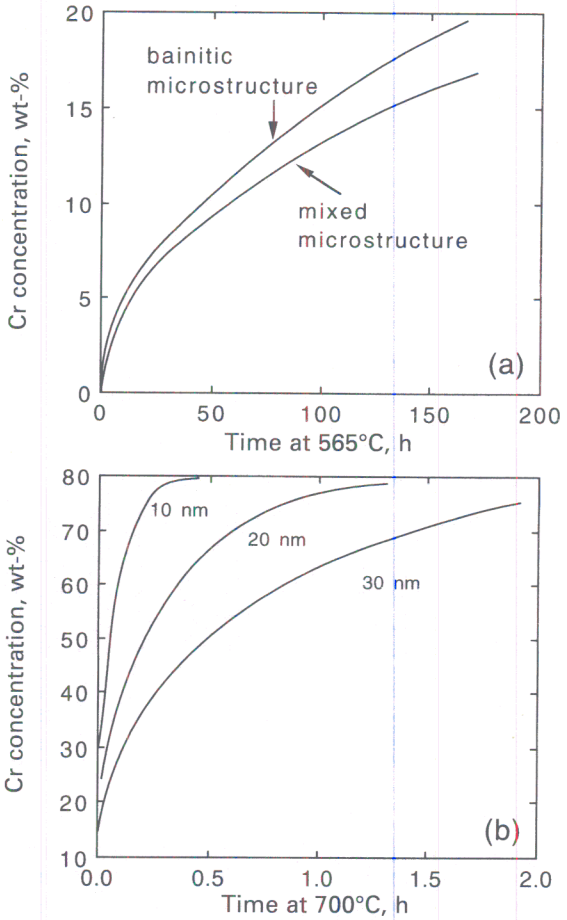

13 *a* 2·25Cr–1Mo steel: cementite enrichment in fully bainitic microstructure and mixed allotriomorphic ferrite and bainite (Refs. 47, 48), and *b* rapid saturation of cementite in 12Cr–1Mo–V steel aged at 700°C, as calculated for various particle sizes (Refs. 50, 51)

after the stress relief heat treatment (typically several hours at 700°C) is cementite. The cementite is very slow to enrich and to convert to alloy carbides, thus allowing the process to be followed over a period of many years during service. As the concentration of carbide forming elements is raised, the kinetics of cementite enrichment and alloy carbide precipitation become more rapid (Fig. 13*b*). Thus, relatively stable alloy carbides tend to dominate the microstructure after short periods in service or even after the stress relief heat treatment.[51] When compared with cementite, the formation of alloy carbides involves considerable diffusion so that they form with a chemical composition which is not far from equilibrium. Changes may nevertheless occur if, for example, the heat treatment before service is at a different temperature when compared with the service temperature, since the carbide must then adjust to an equilibrium consistent with the service conditions.

Figure 14 shows microanalysis data from vanadium rich carbides for two samples with average composition Fe–0·11C–0·3Mn–0·28Mo–0·23V–0·023N wt-%. The 'virgin' sample was produced by tempering at 700°C for an unspecified time period, following normalisation at 950°C for an unspecified period. The

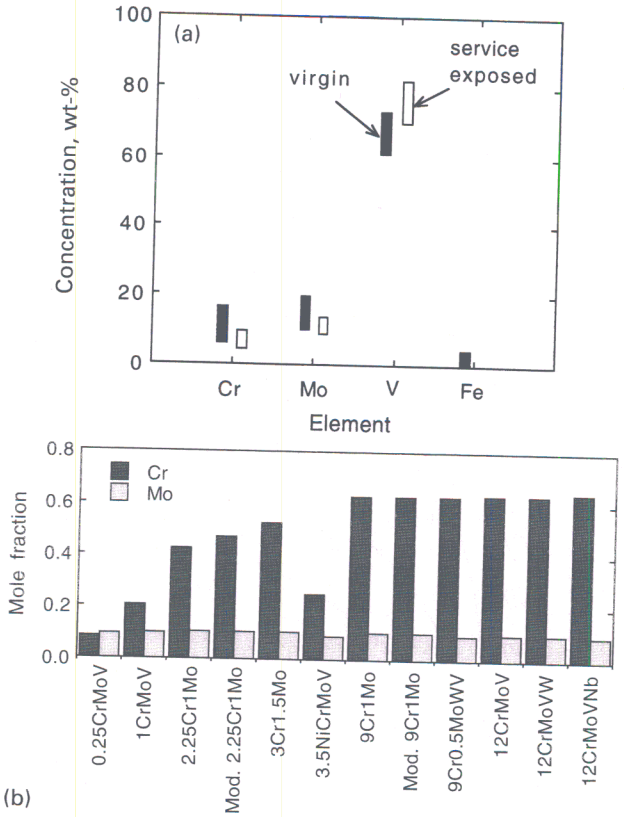

14 ***a*** **chemical compositions of V rich carbides in virgin material (1Cr–0·3Mo–0·25V) and in samples which had been in service for 10 years,[40] and** ***b*** **concentrations of Cr and Mo in $M_{23}C_6$ in power plant steels listed in Table 4 (for 565°C); data calculated using MTDATA program**

exposed sample had in addition spent 10^5 h at 540°C and 50 MPa. There is no significant difference between the carbide compositions from the two samples. There is therefore little prospect of estimating the remaining life of high alloy steels, or of steels in general, by following changes in the chemical compositions of alloy carbides. As a matter of interest, Fig. 14*b* shows the chromium and molybdenum concentrations of the most prominent alloy carbide found in most power plant steels (*see* also Tables 3, 4).

One possibility is to follow the detailed microstructural changes. Figure 15 is a simplified presentation of the evolution of carbide and Laves phases during the aging of a 9Cr–Mo–V–W steel (NF616) which is tempered from its martensitic state at a temperature of 600°C over six orders of magnitude of time. Obviously, an identification of the fractions of the phases could help to fix the state of the steel. Some of the precipitation reactions are sensitive to temperature. For example, the driving force for the precipitation of Laves phases decreases greatly as the temperature increases.

Overall changes in microstructure

The main factor responsible for the good creep resistance of the steels used in the power generation industry is the formation of fine and highly stable

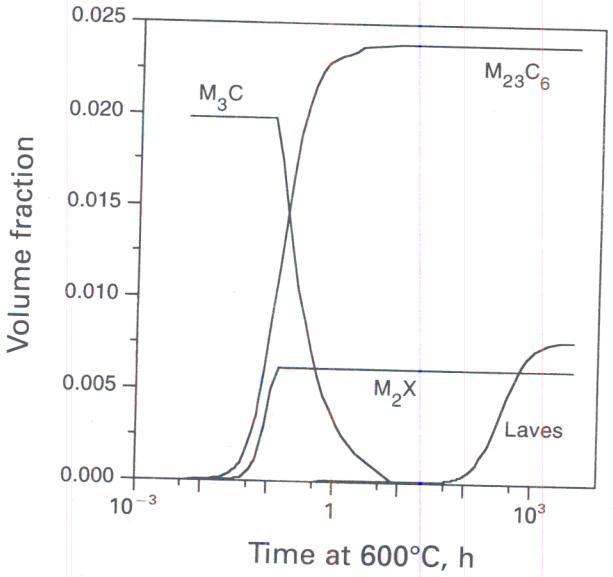

15 Calculated evolution of phase fractions in 9Cr–Mo–V–W steel (NF616) during tempering at 600°C (after Ref. 52)

dispersions of alloy carbides.[53] A significant contribution also comes from solid solution strengthening by substitutional solutes. The solid solution strengthening component becomes more important after prolonged service at elevated temperatures, as the microstructural contribution to strengthening diminishes due to annealing effects.

The heat treatments given to the steels before service are usually so severe that the precipitates are in an overaged condition.[54] The microstructures are therefore relatively stable before service, though further microstructural changes are inevitable given that service involves many decades at temperatures where substitutional atoms have significant mobility. It will be shown that these changes can be used to monitor life.

1Cr–0·5Mo steel

The hardenability of this alloy is marginal so that it can be found in three microstructural states when ready for service: (a) ferrite and pearlite; (b) ferrite and bainite; and (c) a mixture of ferrite, pearlite, and bainite. Cementite and M_2C carbides are also present in the initial microstructure. The changes that occur in the microstructure during service are summarised in Table 7, in terms of the fraction of life expended (t/t_r). Dobrazanski and co-workers[55] have established atlases of microstructure which enable the remaining life to be characterised to an even higher precision than indicated in Table 7.

2·25Cr–1Mo

This steel usually has an upper bainitic microstructure but can contain substantial quantities of allotriomorphic ferrite, especially in large components which have been cooled slowly from the austenitisation temperature. The mixed ferrite/bainite microstructure actually is better in creep because, for reasons which are not clear, M_2C carbide persists

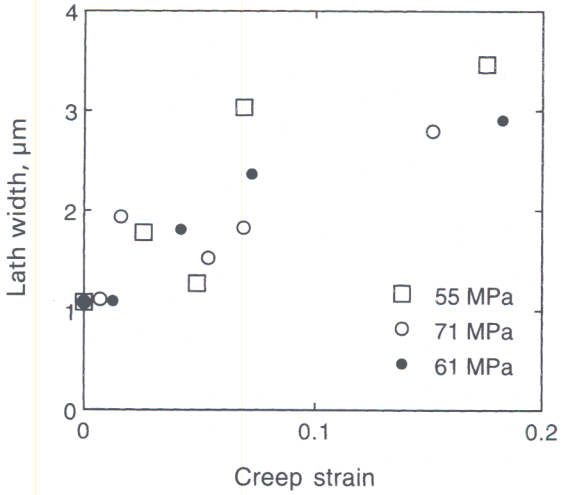

16 Lath size in 2·25Cr–1Mo steel as function of secondary creep strain during tests at stresses indicated; strain measurements have an error of ±0·01 and lath size data an error of ±0·25 μm (after Ref. 56)

longer in ferrite than in bainite or martensite, presumably because the higher defect densities associated with the last two microstructures enhance diffusion rates.

Heat treatment before service involves austenitisation at about 950°C for a time period dependent on the component size (typically several hours), followed by air cooling to ambient temperature. The component is then tempered at 710°C for 16 h to produce a 'stable' microstructure of overaged upper bainite with a prior austenite grain size of about 80 μm. A coarsened lath structure (width ~0·8 μm) is seen using transmission electron microscopy, with $M_{23}C_6$ alloy carbide particles located mainly at the lath boundaries. These particles do not seem to coarsen much during service though there must be an overall coarsening of pinning particles since the lath size is found to coarsen (Fig. 16), though even in this case, the data are restricted to very small strains typical of the early stages of life.

Table 7 Broad microstructural changes as function of life fraction consumed, for 1Cr–0·5Mo steel* (adapted from Ref. 55)

t/t_r	Microstructure
0	Ferrite plus bainite and/or pearlite M_3C and M_2C
0·2	Ferrite and partially disintegrated bainite/pearlite M_3C, $M_2C\uparrow$ and $M_{23}C_6\uparrow$
0·3–0·4	Ferrite and completely disintegrated bainite/pearlite $M_3C\downarrow$, $M_2C\downarrow$, $M_{23}C_6$ and $M_6C\uparrow$
0·4–0·6	Ferrite and coarse carbides $M_2C\downarrow$, $M_{23}C_6$, and M_6C Small number of irregularly spaced isolated cavities
0·6–0·8	As above but more cavities Many cavities coalesced or about to do so
0·8–0·9	As above but cracklike coalescence of cavities
0·9–1·0	Macroscopic cracking (removed from service)

* The observations of ferrite, bainite, pearlite, and cavitation are on an optical microscope scale. The arrows indicate whether the phase concerned is increasing or decreasing with time.

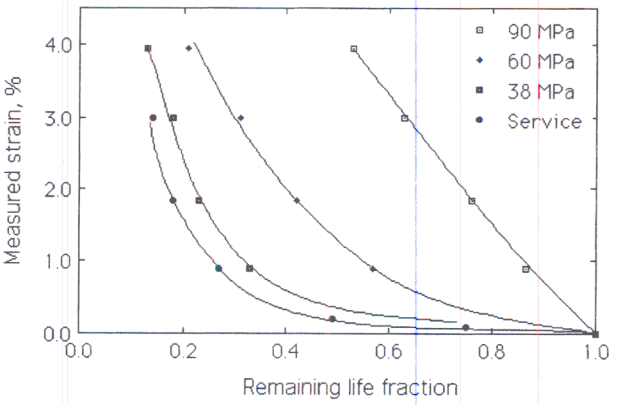

17 Creep strain as function of remaining life; data are for creep samples loaded at three stresses, data marked 'service' refer to conditions for thick walled pressure vessel (after Ref. 57)

Creep strain and rupture data

Strain monitoring

Creep strain is a direct measure of remaining life (Fig. 17) and is a quantity which can be monitored during service using a variety of techniques. It is estimated that to obtain an accuracy of 10% in the predictions of remanent life requires a strain measurement capability of 0·01%. The methods for measuring strain include continuous measurements using strain gauges, discontinuous measurements during maintenance shutdowns, the use of measurement grids plated using noble metal to avoid oxidation, special extensometers and studs welded to the surface as reference marks.[5,6,57] As pointed out by Parker,[57] care has to be exercised to ensure that the distance over which the measurement is carried out is appropriate for the component concerned. For example, a welded joint has an inhomogeneous microstructure; local strains in the heat affected zone may be much larger than the value measured across the whole joint. Notwithstanding these difficulties, it is possible to relate the strain directly to the remaining life using an appropriate model.[31]

In circumstances where the creep data are from short term experiments and hence of small strains, the Evans and Wilshire[1] equation may be used to extrapolate to larger strains ε

$$\varepsilon = \underbrace{\theta_1[1-\exp(-\theta_2 t)]}_{\text{decaying rate}} + \underbrace{\theta_3[\exp(\theta_4 t)-1]}_{\text{accelerating rate}} \qquad (13)$$

where θ_i are obtained by fitting to experimental data, and t is the time at temperature. The first two of these parameters describe the primary or decaying strain rate component, whereas the remaining terms concern the accelerating regime. Parker has used this equation to predict successfully the remaining life of a Cr–Mo–V pressure vessel steel. He also suggests that the number of inspections should be increased once the creep strain has exceeded 1%.

In practice most power plant components are subjected to more complicated stresses than uniaxial tension. Plastic deformation occurs when the shear yield stress τ_y is exceeded. For uniaxial tension, yield-

ing occurs when the principal stress σ_1 reaches the normal yield strength σ_y, which is identical in magnitude to the shear yield strength τ_y. For torsion, the maximum principal stress σ_1 must reach a magnitude $\sqrt{3}\tau_y$ before plastic deformation occurs; this comes from the application of the von Mises yield criterion which can be interpreted to mean that plastic flow occurs when the shear strain energy reaches a critical value (e.g. Ref. 58). It is convenient to use normal rather than shear stresses so plastic deformation is said to occur at an equivalent normal stress σ^*, which for tension is $\sigma^* = \sigma_y$ whereas for torsion $\sigma^* = \sqrt{3}\sigma_y$. This equivalent stress can be calculated for a variety of multiaxial stress systems using the von Mises criterion. The importance of multiaxial stresses in the development of cavitation damage is well established.[59,60] Cane[60] has pointed out that strain monitoring will lead to an underestimation of damage when $\sigma_1/\sigma^* > 1$ and vice versa when $\sigma_1/\sigma^* < 1$. Thus, for the same maximum principal stress σ_1, cavitation damage will be more severe in uniaxial tension than in torsion.[61]

Creep rupture

Naturally, the creep rupture testing of service exposed material is considered to be one of the most reliable ways of estimating the remaining life of a component.[17,18,62] This assumes that test samples can be removed 'non-destructively' from the component and that the samples are reliable. Several samples are required even when reliability is assured, because the tests have to be done at accelerated rates in order to be of use. The data are then extrapolated to the operating conditions in order to estimate the remaining life. Given the material limitations, the samples are usually much smaller in size than is usual in creep testing. The problems associated with the small size are discussed in the section 'Small specimen testing' below; attention is focused here on the analysis of the creep data.

The steady state creep rate $\dot{\varepsilon}$ is in theory given by, e.g. Ref. 3

$$\dot{\varepsilon} = b_3 \sigma^n \exp\left(-\frac{Q}{RT}\right) \quad \ldots\ldots\ldots \quad (14)$$

where b_3 is an empirical constant, Q an activation energy, σ the applied stress, T the absolute temperature, and R the universal gas constant. This equation can be integrated to find the creep rupture time t_r as

$$\ln t_r = \ln\left(\frac{\varepsilon_r}{b_3}\right) - n \ln \sigma + \frac{Q}{RT} \quad \ldots\ldots \quad (15)$$

Nevertheless, it is found in practice that slightly better fits are obtained by writing[60,62]

$$\ln t_r = b_4 + b_5 \sigma + b_6 T \quad \ldots\ldots\ldots \quad (16)$$

where b_4, b_5, and b_6 are fitting constants.

The small sample tests used to derive the constants typically extend over a temperature range 540–675°C and for a time period of 10 000 h. Any relationship for the creep rupture time must therefore be extrapolated to much longer times and service conditions. It has yet to be demonstrated whether the empirical relations extrapolate better than the physical relationship implied in equation (15).

It has been argued that the use of very high temperatures during accelerated testing is unwise since microstructural changes might occur which are not representative of service at lower temperatures.[62] This is based on the fact that the creep rupture data from very high temperature tests exhibit a different behaviour from those at other temperatures in the range studied. Power plant steels are usually heavily tempered before they enter service, for many hours at temperatures in the range 680–750°C, in order to stabilise the microstructure and to relieve stresses. 'High temperature' thus refers to temperatures in the vicinity of the original tempering temperature. It is recommended, therefore, that accelerated creep tests are confined to temperatures some 50 K lower than the original tempering temperature.

Scale formation

When using isostress rupture tests for the prediction of remaining life in boiler components such as reheater tubes, the formation of scale on the steam side of the tube, and the fire corrosion on the other side must be taken into account.[11] Fire corrosion has the effect of reducing the thickness and hence of increasing the stress on the remaining section. The buildup of scale on the other hand leads to a continuous increase in the temperature of the tube by insulating the inner surface. Any calculations therefore require a knowledge of the rate of oxide formation (and hence of tube temperature increase) and of fire corrosion (and hence of stress increase), both of which can be incorporated into an assessment using an appropriate life fraction rule. In the absence of oxide spalling, the current thickness of the oxide can be used to assess the effective temperature using experimental data of the kind illustrated in Fig. 18 for 2·25Cr–1Mo steel.

Creep ductility

The ability of a material to tolerate strain is important because it determines whether the failure occurs gradually with some warning, or whether it is sudden. The latter scenario is less desirable and would require a greater safety factor in design or in any life assessment. It is strange that many design criteria do not include a consideration of the rupture ductility.[5,6]

The reasons why creep ductility varies so much in practice are not well established. The variation can be from 2 to 30% in conditions which are nominally identical.[62] Contributing factors include residual elements, grain size, inclusions, solution treatment, and tempering treatments, etc. With small ductilities, cavitation can be detected at correspondingly smaller strains (as low as 0·5%) whereas higher ductility components do not reveal signs of cavitation with strains as large as 5% (Ref. 64).

It appears that many alloys show a creep ductility minimum as a function of the test temperature and service period. The life assessment should therefore be made bearing in mind the relationship between the service temperature and that at which the ductility minimum occurs. For 1Cr–Mo–V steel, the minimum occurs between 5000 and 30 000 h at 550°C (Ref. 62).

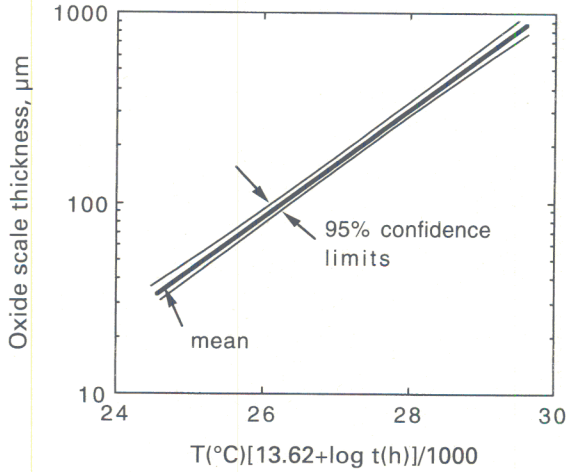

18 Oxide thickness for 2·25Cr–1Mo steel in steam at 538–593°C as function of Larson–Miller parameter (after Ref. 63)

Cavitation damage

It has already been noted that cavitation occurs in steels that are relatively brittle in creep and in regions where there is a concentration of stress. In fact, deformation by creep is far from homogeneous even on a microstructural scale. One manifestation of this is the formation of cavities at the grain boundaries between differently oriented crystals. The boundaries contain incoherent particles, primarily sulphides, which can decohere and provide the sites where cavities generally form.[65] Cavitation plays a critical role in the events leading to ultimate failure and hence is a direct measure of remaining life.

The cavities tend to form mostly on boundaries with normals parallel to the principal tensile stress by a process of nucleation and growth, though damage also occurs on inclined boundaries if the applied stress is large.[60] Thus, at any instant of life, only a fraction of the transverse boundaries have cavitation damage. There are constraints to cavity formation when only some of the transverse boundaries are cavitated, and this has important consequences on the creep rupture life.[66] In Fig. 19*a*, all the transverse boundaries have identical cavities. The regularity of the structure allows the cavities to grow unconstrained, the extension along the stress axis being accommodated by grain boundary sliding. This is not the case when, as illustrated in Fig. 19*b*, only some of the boundaries have cavities. The extension due to the cavities at w–x results in sliding which causes the adjacent grains to overlap at y–z. This matter in the shaded region at y–z must be carried away by diffusion before the cavities at w–x can continue to grow. This in effect imposes a constraint on the growth of the cavities when compared with the situation in Fig. 19*a*. The physical basis of the retardation is that cavity growth now becomes controlled by the rate of matrix creep. The retardation is very significant, as seen in Fig. 19*c*.

A parameter

One method of characterising cavitation is the '*A* parameter' determined as the number fraction of

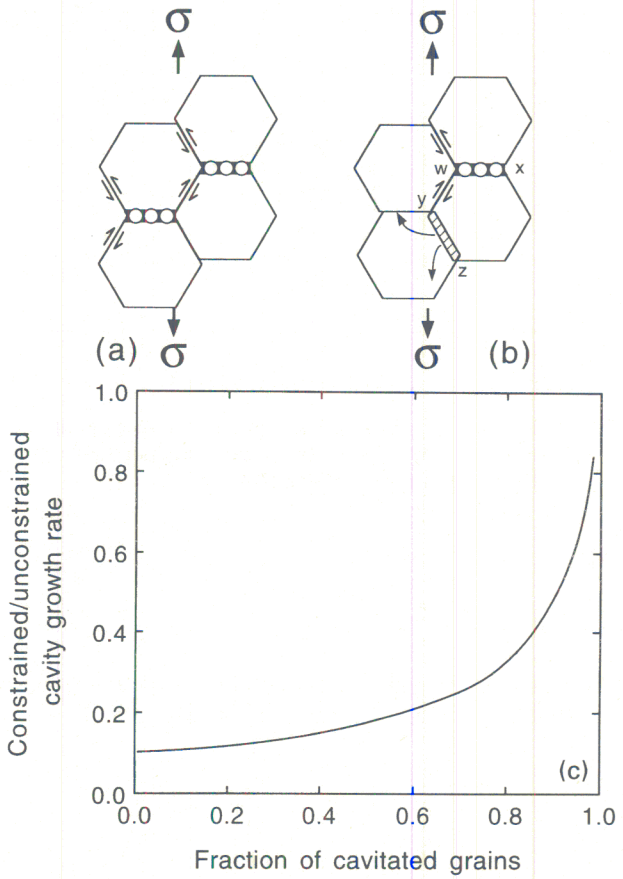

a all transverse boundaries cavitated; *b* non-uniform cavitation; *c* reduced cavity growth rate when cavitation is not uniform

19 Effect of constraint on growth rate of cavities (after Ref. 66)

cavitated grain boundaries traversed by a scan parallel to the stress axis of a creep test specimen, whilst avoiding the necked region. The method presented below is due to Shammas[67] and relies on the assumption that any cavitated boundary is one which can be considered to have been completely damaged and incapable of supporting load. The creep rate as given by equation (14) therefore becomes

$$\dot{\varepsilon} = \frac{b_7 \sigma^n}{(1-A)^n} \quad \ldots\ldots\ldots\ldots\ldots\ldots (17)$$

where the term in the denominator accounts for the increase in stress due to a reduction in the cross-sectional area as a fraction A of the boundary normal to the stress becomes unavailable to support the load; b_7 is an empirical constant. This might be a reasonable assumption because it is well known that a boundary is severely damaged on a fine scale once cavities become optically visible.

If it is now assumed that

$$\dot{A} \propto \frac{1}{(1-A)^{b_8}} \quad \ldots\ldots\ldots\ldots\ldots\ldots (18)$$

where b_8 is an empirical constant. Since $A = 0$ at $t = 0$ and $A = 1$ at $t = t_r$, the integration of equation (18) gives

$$(1-A) = \left(1 - \frac{t}{t_r}\right)^{1/(b_8+1)} \quad \ldots\ldots\ldots\ldots (19)$$

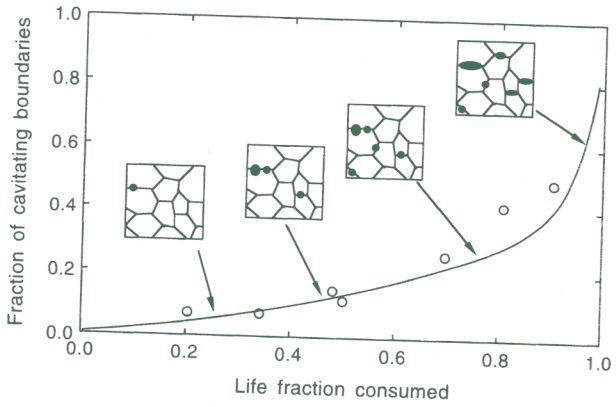

20 Fraction of cavitating grain boundaries as function of life fraction consumed for 2·25Cr–1Mo steel (after Ref. 67)

so that

$$\dot{\varepsilon} = b_7 \sigma^n \left(1 - \frac{t}{t_r}\right)^{-[n/(b_8+1)]} \quad \ldots\ldots\ldots \quad (20)$$

This can be integrated subject to the conditions that $\varepsilon = 0$ at $t = 0$ and $\varepsilon = \varepsilon_r$ at $t = t_r$, giving

$$\left.\begin{aligned} \frac{\varepsilon_r}{\varepsilon} &= \left(1 - \frac{n}{b_8+1}\right)^{-1} \\ \text{and} \\ \left(1 - \frac{t}{t_r}\right) &= \left(1 - \frac{\varepsilon}{\varepsilon_r}\right)^{\lambda} \end{aligned}\right\} \quad \ldots\ldots \quad (21)$$

where $\lambda = \varepsilon_r/\varepsilon$. Comparison with equation (19) gives

$$A = 1 - \left(1 - \frac{t}{t_r}\right)^{[1-(\varepsilon/\varepsilon_r)]/n} \quad \ldots\ldots\ldots \quad (22)$$

where as usual, t_r is the time to rupture, ε the creep strain, ε_r the creep rupture strain, and n a fitted constant. Any strain during primary creep is neglected. Figure 20 shows both experimental data and a curve calculated using equation (22) and assumed values of $\varepsilon_r/\varepsilon = 2{\cdot}5$ and $n = 3$ (Ref. 67). The data seem to follow the form indicated by the equation but there are other results[19,68] which suggest that the relationship remains linear up to the point of life exhaustion, though the degree of scatter in the A parameter increases significantly for life fractions greater than 0·96.

The A parameter is defined in terms of the number fraction of transverse boundaries which are cavitated. Many models for creep associate fracture with a complete loss of area available to support the load as the cavities coalesce along the appropriate plane.[69–71] A strict measure of the damage would then be the area fraction of transverse boundaries that is decorated by cavities. The A parameter, on the other hand, could reach unity before the transverse boundaries are completely detached. However, this may not be a problem in practice if the rate of damage increase in the final stages is very high.

The magnitude of the A parameter at failure, i.e. A_r, is found to vary considerably with the test temperature, applied stress, creep ductility, and austenite grain size though it is emphasised that these variables

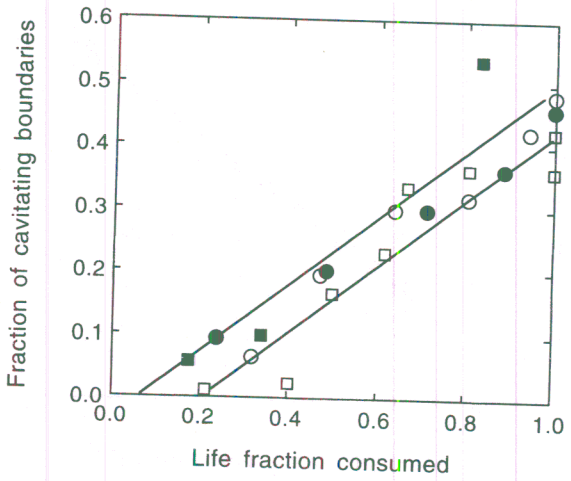

21 Changes in A parameter as function of expended life fraction in 1Cr–0·5Mo steel tested at 550°C: solid symbols represent commercial purity steels and open symbols high impurity steels; squares are data acquired from interrupted tests on single specimens whereas each circle is from different sample (after Ref. 11)

may not all be independent. For example, A_r increases as the test temperature decreases towards the ductility minimum for the steel concerned. For 1Cr–Mo–V type steels, A_r decreases from about $0{\cdot}20 \pm 0{\cdot}1$ to $0{\cdot}02 \pm 0{\cdot}02$ as the elongation to failure increases from 2 to 33%.[72] The scatter in A_r is reduced, but only slightly, when the experiments are confined to just one steel. Similarly, A_r varies from about $0{\cdot}07 \pm 0{\cdot}05$ to $0{\cdot}35 \pm 0{\cdot}05$ as the prior austenite grain size changes from 22 to 75 μm. This latter effect may also be related to variations in creep ductility, which is dependent on the austenite grain size.

Cavity formation and creep deformation are sensitive to impurities in the steel and this might be reflected in the measured values of the A parameter. Viswanathan[11] has compared high purity and commercial purity 1Cr–0·5Mo steels but there are no systematic trends within the scatter inherent in the measurements (Fig. 21). Similarly, it does not seem to matter whether the cavitation measurements are done by interrupting a single test or by using a series of specimens.

The A parameter is considered to be of little use in life assessment when the creep ductility is greater than about 5% (or austenite grain size less than about 25 μm).[72] This is because such materials are unlikely to exhibit creep damage during the course of safe service, the damage setting in at a stage close to failure. For steels with low creep ductility and large austenite grain size, the A parameter can be used to assess life fraction since changes in A can be observed as a function of life fraction. Measurements like these for 1Cr–Mo–V rotors indicate that the absence of any observable creep cavitation indicates a minimum remaining life fraction of ~0·45 (Ref. 72). This obviously is steel and technique specific because work on 1Cr–0·5Mo steels tested at 550°C shows that about 60% of the life remains at a stage when isolated cavities are discovered in the (optical) microstructure

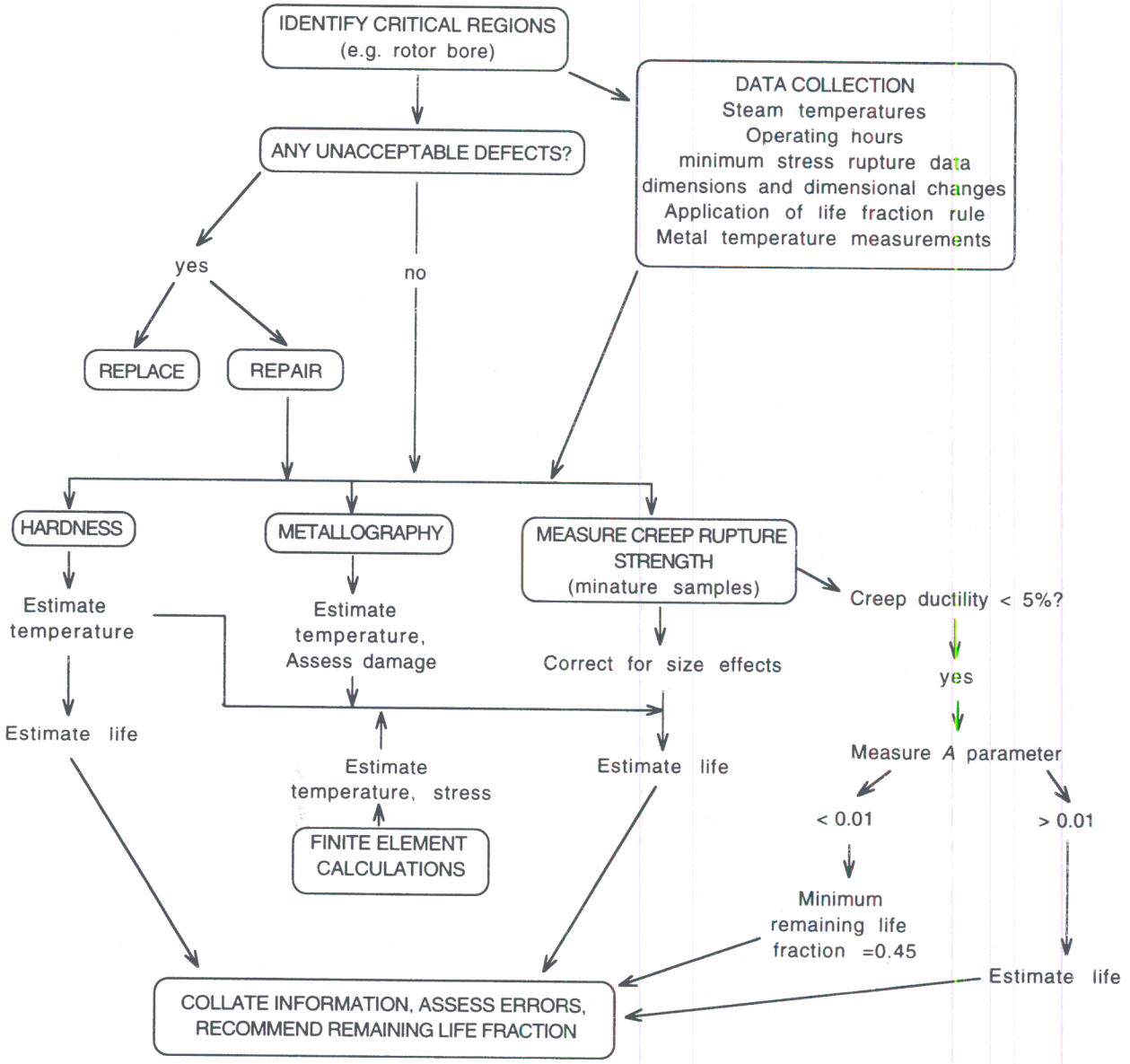

22 General procedure which has been used to assess remaining life of rotors

using a replica technique.[11] A general procedure used successfully in the assessment of the remaining life of 1Cr–Mo–V rotors is shown in Fig. 22.

Another method of assessing the remaining life using cavitation damage involves the measurement of the number density of cavities, which seems to increase in proportion to the creep strain during uniaxial loading.[56,59,73,74] This may not in fact amount to a different method (compared with the A parameter) in the context of steels where the important cavities tend to form at the grain boundaries. The proportionality between the cavity population and strain is limited to small strains (up to 0·2). Deviations occur at large strains because some contribution to the creep strain comes from general deformation and also because the cavity nucleation sites become exhausted at the late stages of creep life.

The volume fraction of cavities increases approximately with the strain and can be used as a measure of remaining life,[71] though differences in the distribution of cavities (due to differences in microstructure) could introduce variations in creep life at constant cavity fraction.

Qualitative methods

There are several general classifications of creep cavitation damage. Thus, Neubauer and co-workers[75,76] have categorised damage into the following categories based on optical microscope observations: no detectable damage; isolated cavities; oriented cavities*; linked cavities (microcracks); and macrocracks about the size of a grain. Significant action is considered necessary, in the form of inspections, when oriented cavities (strings of cavities on boundaries normal to the stress axis) form and repair begins when the cavities begin to link. Macrocracks are of course, unacceptable and must be repaired immediately.

As pointed out by Strang *et al.*,[17] these and more sophisticated qualitative classifications are useful in

* Meaning that there is an alignment of damage normal to the maximum principal stress.

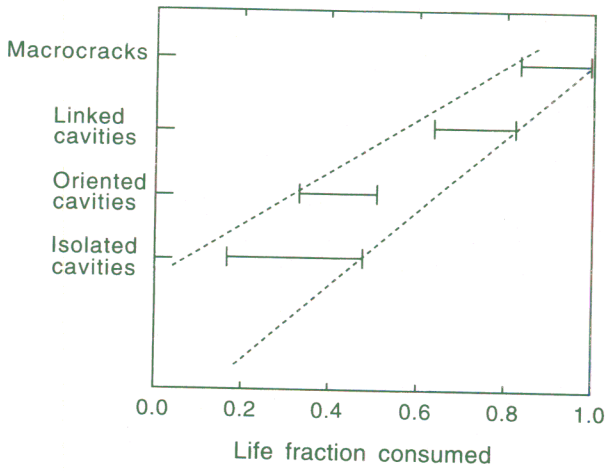

23 Correlation between cavity classifications and life fraction consumed for 1Cr–0·5Mo steels tested at 550°C; data are for high purity and commercial purity steels (after Ref. 11)

defining the safe service inspection intervals but not necessarily in the estimation of the remaining life for a given component. The prediction of life requires quantitative rules which give conservative estimates when extrapolated. On the other hand, the quantitative rules must take into account the heterogeneous nature of cavitation damage so that field parameters such as the cavity fraction are not on their own sufficient. Viswanathan[11] has proposed a compromise by linking the observations to direct measurements of the creep rupture life. His data for 1Cr–0·5Mo type steels are illustrated in Fig. 23, where the Neubauer categories are plotted against the expended life fraction measured using creep rupture tests. The rate of cavitation damage in this case seems more severe than indicated in Table 7.

One important use of purely qualitative classifications is that they help in establishing a methodology which allows a comparison between different research groups. Wu *et al.*[77] have developed a detailed classification of cavitation damage, which can readily be reduced to the Neubauer categories (Table 8). A variety of similar classifications have been incorporated in European guidelines for in service damage assessment, for example, NORDTEST NT TR170 and VGB–TW507.

Techniques for measurement of cavities

Optical microscopy is frequently used to examine longitudinal sections from creep test specimens and the main difficulties during such examinations is the possibility of confusing cavities and localised pitting or boundary carbides unintentionally extracted from the sample surface. Therefore, one procedure is to use standard metallographic polishing to 6 μm diamond finishing. This is followed by repeated polishing with γ-alumina[56] or 1 μm diamond polish[72] and light etching in 2% nitric acid in methyl alcohol. This procedure minimises surface deformation effects which might obscure cavities. Reproducible results are obtained as long as these preparation conditions are standardised. However, the results from any technique must depend on resolution. It is well known that scanning electron

Table 8 Damage ratings developed by Wu *et al.*[77] with experiments on rolled seamless pipes of 220 mm outer diameter and 20 mm wall thickness*

Rating	Appearance of cavitation
1	No cavities
Isolated cavities	
2B	1–100 cavities mm^{-2}
2C	100–1000 cavities mm^{-2}
2D	$\geqslant$1000 cavities mm^{-2}
Strings of cavities	
3B	Few strings and isolated cavities 2B
3C	Few strings and isolated cavities 2C or 2D
3D	Numerous strings and isolated cavities up to 2D
Microcracks $\leqslant$0·1 mm	
4A	Reheat cracks*
4B	Few microcracks and damage 2B or 3B
4C	Few microcracks and damage 2C, 2D or 3C, 3D
4D	Numerous microcracks and damage 2C, 2D or 3C, 3D
Macrocracks $\geqslant$0·1 mm	
5A	Reheat cracks*
5B	One macrocrack ($\leqslant$1 mm) and damage 2B, 3B, or 4B
5C	Macrocracks ($\leqslant$5 mm) and damage 2C, 3C, or 4C
5D	Macrocracks ($\leqslant$5 mm) and damage 2D, 3D, or 4D, or creep crack (>5 mm)

* 'Reheat cracking' occurs by cavitation on grain boundaries in the coarse region of the heat affected zone of a weld. It requires a matrix which is strong (strengthened, for example, by fine vanadium carbides) due to an inadequate heat treatment after welding, a precipitate-free zone at the boundaries and impurity particles (MnS) at the boundaries which help nucleate cavities.[5,6,78]

microscopy of intergranularly fractured specimens exposes cavitation at a much smaller overall strain than is apparent using optical microscopy.[56]* High voltage transmission electron microscopy can reveal even finer dispersions of cavities; observations like these have confirmed the tendency for cavities to form preferentially at carbide particles. The cavities also appear to be crystallographically faceted.

Many measurements are made on samples which are creep tested in air. It is then important to avoid heavily oxidised surface regions and regions where necking (intense localised deformation) has occurred. Strang *et al.*[72] therefore conducted measurements in the central two-thirds region of the sample gauge length, keeping one gauge diameter away from the fractured surface. The samples are examined on their central longitudinal sections containing the tensile axis.

Cavitation damage methods also depend on a clear identification of the prior austenite grain boundaries, which can be difficult in heavily tempered ferritic microstructures.[72]

Fracture toughness

It is well established that the fracture toughness of many power plant steels deteriorates during service for two reasons. First, the carbide particles, particularly those located at boundaries, coarsen and hence provide easier sites for crack or void nucleation. Second, the segregation of impurities to interfaces has an opportunity to proceed to its equilibrium extent during service. The rate of this embrittlement can sometimes be modelled.[79]

* Intergranular fracture can be promoted by fracturing the samples at liquid nitrogen temperature.

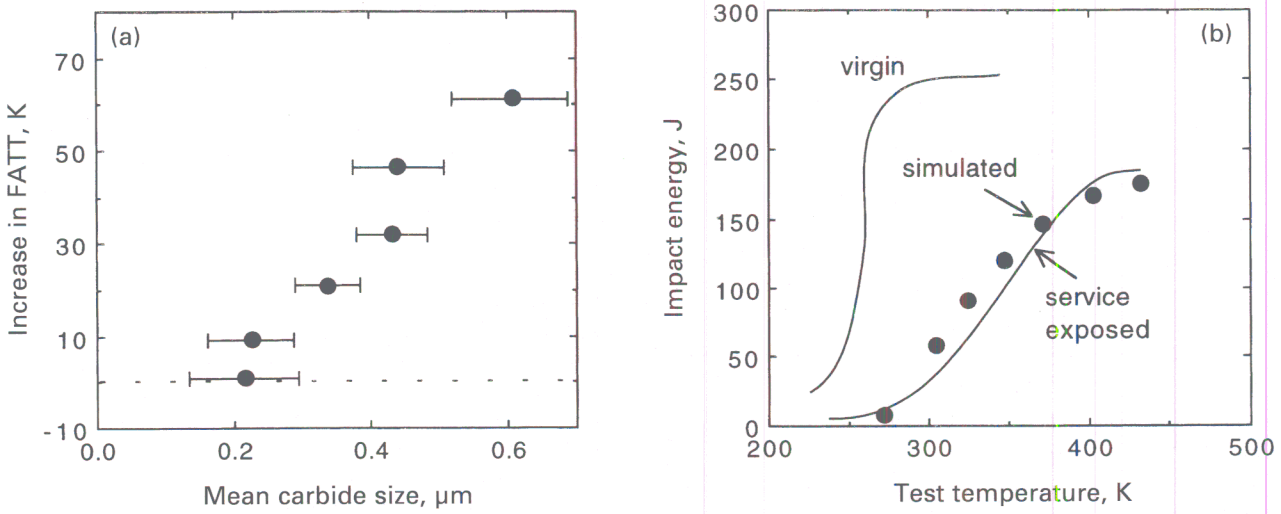

a change in fracture appearance impact transition temperature (FATT) with mean carbide size as function of aging; *b* comparison of impact energies of steel in its virgin condition after exposure service at 813 K for 88 000 h and for service simulated sample (873 K for 10 000 h)

24 Impact test data for 2·25Cr–1Mo steel (after Ref. 80)

The tendency to embrittle during service is sometimes simulated by an accelerated step cooling experiment in which the sample is held at a variety of decreasing temperatures over the embrittlement range, and then allowed to cool to ambient temperature at a very slow rate. Unfortunately, though the procedure does allow the sensitivity of the sample to embrittlement phenomena to be tested, the data can not be used to discover the state of the steel in its aging process (a remaining life assessment).

Figure 24*a* shows how the fracture appearance transition temperature (FATT) assessed from impact tests varies with the mean carbide particle size in a 2·25Cr–1Mo steel.[80] Figure 24*b* shows the complete transition curves for both the virgin steel (i.e. at implementation into service) and for an ex-service sample which had experienced 88 000 h at 813 K. The points represent samples of virgin steel subjected to 873 K for 10 000 h in an attempt to simulate prolonged service at 813 K. These conditions were chosen in order to achieve the same Larson–Miller parameters for the ex-service and simulated samples. It is clear that the agreement between the simulation and service exposed steel is excellent, allowing the method to be added to the panoply of tools available for remaining life assessment.

Misorientation measurements

It is well known from cold deformation experiments that once a dislocation cell structure is established, further strain leads to a decrease in the cell size and a corresponding increase in the crystallographic misorientation between adjacent cells.[81] Dislocations move and their density and distribution also change during the course of creep deformation. These changes are more complex than those associated with cold deformation since there are interactions with precipitates which are deliberately there to interfere with dislocation motion. Nevertheless, it has been known for some time that the orientation between adjacent cells in bainite at first changes linearly with the creep strain as shown in Fig. 25;[56] these measurements were for a 2·25Cr–1Mo steel. The data are limited to rather small strains and hence to the very early stages of service life. Similar results have been reported for creep in aluminium.[82]

Measuremens have also been reported for a ferrite–pearlite microstructure in 2·25Cr–1Mo steel.[83] When compared with bainite, the scale of this microstructure is much larger. The measurements therefore refer to the minute misorientations that develop between dislocation cells within individual ferrite grains over a scale of about 10 μm. This contrasts with the orientation differences between adjacent laths of bainite, which are over distances less than 1 μm. The data for the ferrite/pearlite microstructure are strictly intragranular. Care has to be taken to avoid distortions due to thin foil preparation for transmission electron microscopy. For the same reason, it is recommended

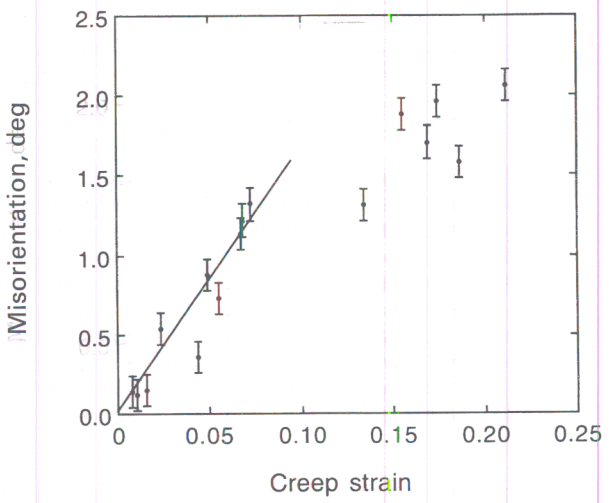

25 Crystallographic 'misorientation' between adjacent laths of bainite in 2·25Cr–1Mo steel as function of secondary creep strain; samples were tested at various stresses and temperatures (after Ref. 56)

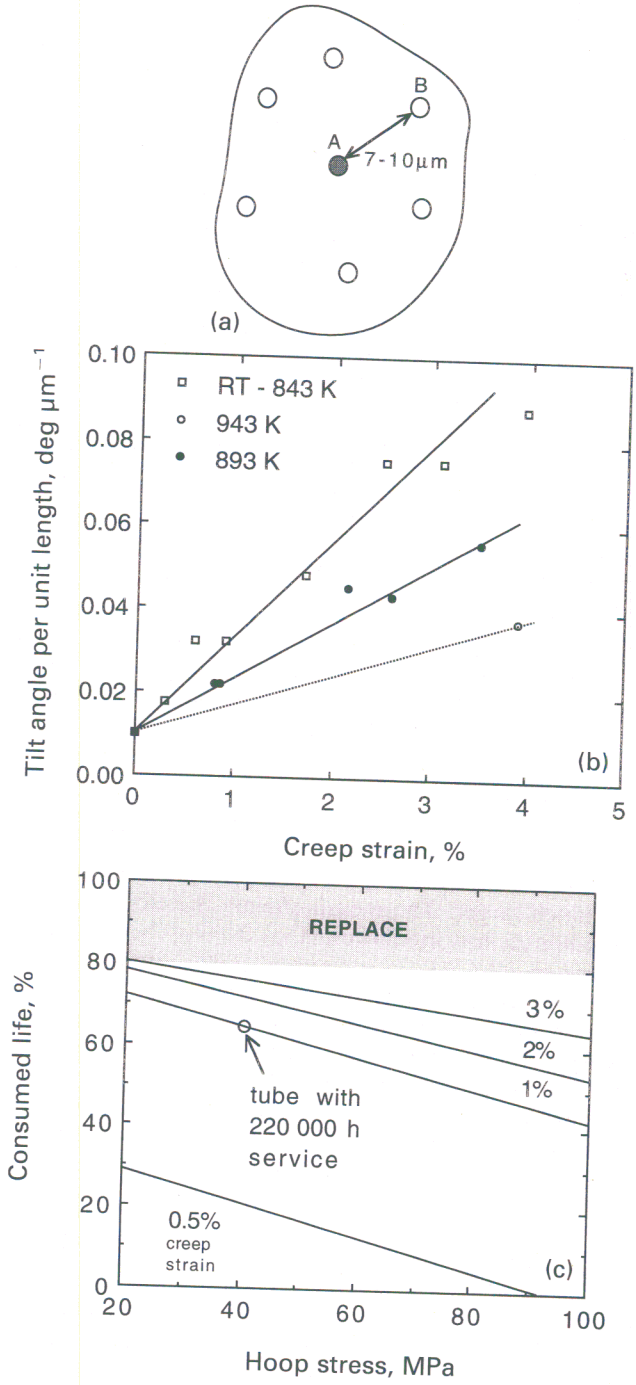

26 ***a*** **measurement of misorientation,** ***A*** **is reference point surrounded by six other points** ***B*** **where relative misorientations are measured;** ***b*** **'misorientation per unit length' for 2·25Cr–1Mo steel tested at various stresses and temperatures as function of creep strain, data are from accelerated tests in which either stress or temperature was increased; and** ***c*** **relation between creep strain and consumed life for heat exchanger tube (after Ref. 83)**

that the orientations are measured in the thick regions of the sample using Kikuchi lines. Figure 26*a* shows the method used, in which the misorientation is defined as the mean of six measurements taken around a reference point. The misorientation is then divided by the distance between the points, and the mean from four repetitions is taken for comparison against overall creep strain.

The accelerated test data illustrated in Fig. 26*b* indicate that the misorientation per unit length increases with increasing creep strain, though there is a strong dependence on the temperature. Thus variations in stress led to the same trend whereas variations in temperature led to different slopes. This is because recovery effects are more prominent at higher temperatures.[83] Accelerated tests are, in the context of misorientation measurements, best conducted with exaggerated stresses. Figure 26*c* shows how misorientation measurements were used to fix the level of creep strain in an ex-service heat exchanger tube, enabling its remaining life to be estimated using design curves.

A rigorous expression of the orientation relationship between identical crystals involves three degrees of freedom, the right-handed angle of rotation, and the three direction cosines of the axis of rotation (only two of the direction cosines are independent since their sum of squares is always unity). A measurement of the angle on its own is not enough. The bcc structure has a high symmetry which means that each axis–angle pair can be expressed in 24 crystallographically equivalent ways. Thus, a 5° rotation about [1 0 0] is approximately equivalent to a 3·5° rotation about [$\bar{1}$ 0 1]. It is surprising therefore that the data in Fig. 26*b* exhibit quite rational patterns.

Hydrogen and remaining life

2·25Cr–1Mo steel is used routinely in chemical plant for pipes carrying hydrogen at about 4 MPa and 530°C. The hydrogen is there as a molecular gas H_2 and hence is not to be confused with nascent hydrogen which is detrimental to steel.

Experiments[84] indicate that this kind of exposure, for a period as long as 135 000 h, appears to have no effect on the creep rupture strength of the steel when compared with virgin samples which have not seen service (Table 9). This is surprising, because even if any potential effect of hydrogen can be neglected, the ex-service material does not appear to have significantly degraded. Measurements of creep strain (Fig. 27) seem to confirm these observations. One possibility is that degradation at 530°C is too slow when compared with the higher temperatures (~565°C) that 2·25Cr–1Mo steel is normally used at.

Bild *et al.*[84] also found that the creep strain of samples which were annealed at 600°C for 1000 h in

Table 9 Creep rupture strength of 2·25Cr–1Mo steel in ordinary tests (A) and for samples which had been exposed to molecular hydrogen at 3·5 MPa for 135 000 h at 530°C (B) (Ref. 85)

Temperature, °C	Time, h	Creep strength (A), MPa	Creep strength (B), MPa
525	30 000	123	129
	100 000	98	92
550	30 000	90	89
	100 000	69	64
575	30 000	65	65
	100 000	48	48

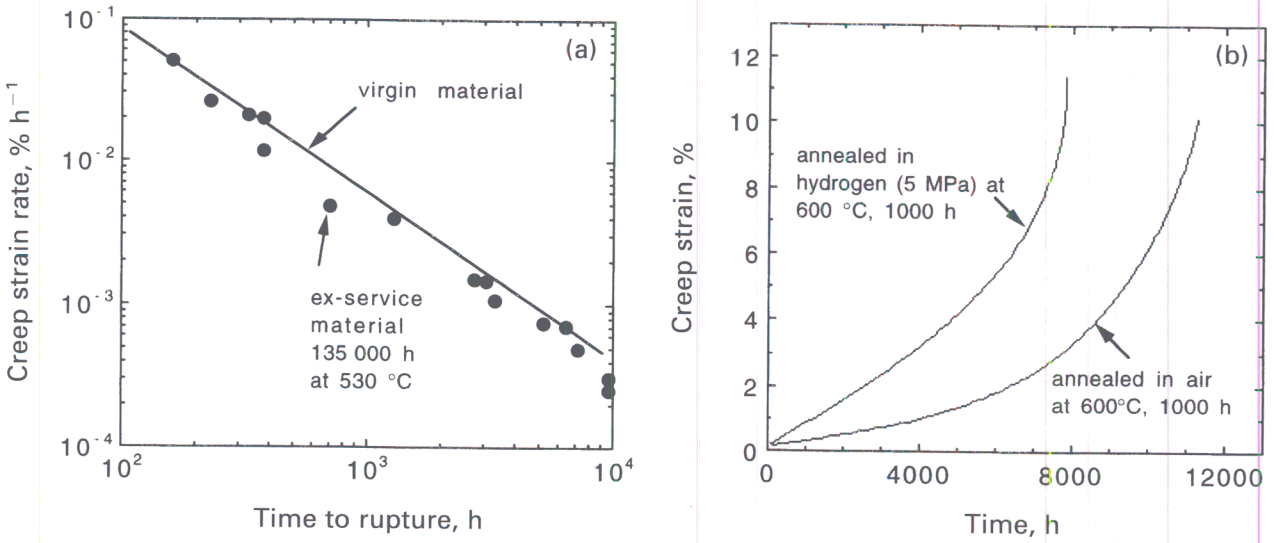

27 ***a*** **minimum creep strain rates of 2·25Cr–1Mo steel in ordinary tests (line) and for samples which had been exposed to molecular hydrogen at 3·5 MPa at 530°C for 135 000 h (points), and** ***b*** **creep curves for 70 MPa at 575°C of samples which were first annealed at 600°C for 1000 h in hydrogen (5 MPa) or in air (after Ref. 85)**

very high pressure hydrogen (5–25 MPa) was significantly greater than those which were similarly annealed in air (Fig. 27*b*). Scanning electron microscopy indicated that the effect of the hydrogen was to eliminate some unidentified fine precipitates from the microstructure, which would be consistent with a deterioration of creep properties. However, both the mechanism of the change in precipitation, and the reason why ex-service material compares well with virgin material (Table 9) remains to be clarified.

Ultrasonics

Ultrasound refers to frequencies up to about 20 MHz. Its penetration into metals leads to a number of effects which can be utilised to detect creep cavitation or microcrack damage. The advantage of ultrasound methods is that they are non-destructive, rapid, and can be used on site.

The introduction of cracks or cavities changes the compliance of the sample and hence must modify the velocity of the sound. However, the effect is so small (about 1% change) that it can not be used with confidence especially when the scatter in experimental data is taken into account.

In a typical ultrasonics test, a spectrum of waves from a probe at the surface propagate through the sample. The waves interact with the metal and are eventually reflected from the opposite side and detected as echoes at the receiver. There are two major echoes, the first from high frequency components and the second from low frequency components. The former is attenuated by defects to a much greater extent than the latter and hence can be used to detect damage (Fig. 28*a*). Nakashiro *et al.*[86] point out that in spite of the acceptable sensitivity of the method, the attenuation tends to be sensitive to the quality of contact between the probe and the sample, and indeed to sample size and geometry, making it difficult to apply in practice.

Nakashio *et al.* propose instead a method based on the analysis of high frequency noise which precedes the arrival of the first backwall echo. The noise in the absence of defects is first defined from a spectrum (decibels dB *v.* frequency) obtained using a defect free sample. The noise is the area of the spectrum in units of MHz·dB. The area measured from a damaged sample is then reduced by the noise associated with the defect free sample to define a noise parameter N, which appears very sensitive to damage (Fig. 28*b*). The method has the additional advantages that it is free from the effects of the inner surface since it does not rely on backwall echoes, and it can be optimised over the high frequency range. It has been used, for example, to characterise the damage in 2·25Cr–1Mo welded samples where there is intense damage in the heat affected zone, leading to the famous Type IV cracking.

Small specimen testing

An excellent review has been published on small specimen tests in the context of irradiation effects, by Lucas.[87] Specific details relevant to the power plant industry are discussed below, but it is worth emphasising some general features highlighted by Lucas. Small samples require a higher standard of machining because they may be more sensitive to surface defects from punching or machining operations. Some creep tests are done on tubular samples which are pressurised, in which case variations in wall thickness can lead to substantial differences in hoop stress. The machining tolerances have to be much better than for large samples. The chances of finding inclusions or other similar defects are reduced with small size specimens and this must be taken into account if scatter is an important issue, or if the property measured is sensitive to inhomogeneities. An obvious example in the latter context is the Griffith crack. Small specimens are also more susceptible to changes in temperature during the course of an experiment.

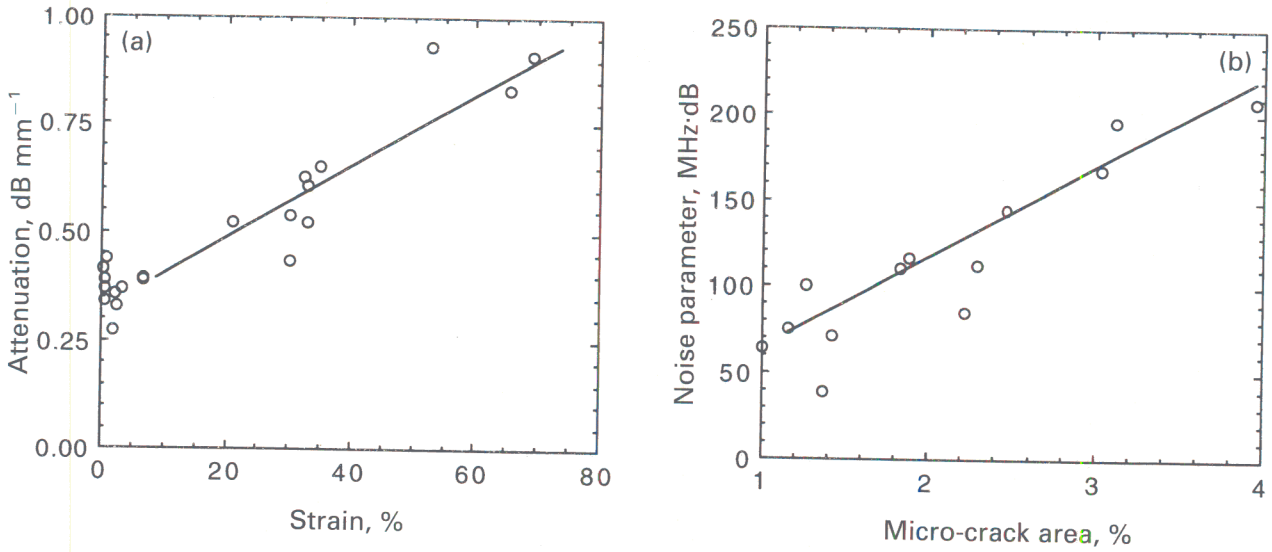

28 ***a*** **relation between attenuation and creep strain for 2·25Cr–1Mo steel, and** ***b*** **relation between microcrack area and noise for 321 stainless steel creep specimen using 30 MHz probe (after Ref. 86)**

Creep tension tests

Miniature, cylindrical creep specimens can be as small as 2 mm dia. and about 4 cm in total length (about 2 cm gauge length). It is also possible to use shorter samples with electron beam welded threaded grips. This compares with normal samples, which are typically 15 mm dia. and 100 mm long. Normal creep tests are conducted in air but the small samples have to be tested in an inert environment (e.g. high purity, dry argon) in order to avoid overwhelming oxidation. The results from small samples tested in this way are typically found to be about 25% better than those from large samples tested in air. This is because of the absence of oxidation, which not only reduces the effective cross-section but the surface oxide can penetrate along grain boundaries leading to notch effects.[62] These effects have to be taken into account when applying small sample data to life assessment procedures.

Many miniature creep rupture tests with 2 mm dia. specimens are conducted in air. Not surprisingly, it has been demonstrated in these tests that the full scale samples last some two to three times longer than the miniature samples.[11]

It is worth noting here that the ISO stress rupture data are based on tests conducted in air. The data are known to underestimate the actual life of thick components where surface oxidation effects matter less.

Bulge tests

Bulge tests rely on parallel-sided sheet samples which are carefully machined from the surface of a component.[87,88] A typical sample would be 8 mm dia. and 0·5 mm thick. Naturally, any high temperature tests must be conducted in inert gas given the rather small thickness. There are two kinds of test, one which is rather like the Ericsson cupping test in which a constrained or unconstrained blank is deformed by a punch with a hemispherical end. The punch moves into a die whose hole diameter is greater than the combined thickness of the punch and 2 × sheet thickness. The second method involves a shearing of the sheet along the punch/die interface; the punch in this case is flat ended and has a cylindrical geometry. Because the deformation is localised when compared with the bulge test, the punch load *v.* displacement curve has characteristics akin to a tensile test. For example, the maximum in the load correlates with the ultimate tensile strength.

Purmenský and Wozniak[88] have applied the method to an unspecified 'Cr–Mo–V' power plant steel to determine the yield and tensile strengths, and some creep properties. It is not completely clear from their work whether the measurements are directly related to bulk properties or whether they have to be converted using calibration experiments. There has been a lot of work on modelling the deformation using finite element and other methods,[87] but inputs such as the punch/sample friction make the extraction of fundamental data quite difficult.

Tensile tests

It is generally agreed that the average yield strength can be accurately assessed using miniature specimens as long as the smallest sample dimension is still much greater than the grain size of the microstructure. The size effect relative to the grain structure is expected since single crystal deformation has different constraints when compared with polycrystalline materials where the grains must deform in a manner which maintains continuity. The required number of grains to produce representative deformation is believed to be about 10–25 (Ref. 87). There may be differences in the level of scatter observed for large and small samples.

It has been known for a long time that the elongation and other measures of ductility are sensitive to specimen geometry and absolute size. Elongation, which is quoted as the sum of uniform and non-uniform deformation, is measured over a gauge length and hence must be geometry dependent. Barba's law[89] expresses the non-uniform component of elongation

as

$$\text{non-uniform elongation } \% = 100\beta \frac{A_O^{1/2}}{L_O} \qquad (23)$$

where L_O is the gauge length, A_O the cross-sectional area, and β an empirical constant with a value of about 1·239. Many testing standards therefore state that the gauge length should be $5{\cdot}65\sqrt{A_O}$. The ultimate tensile strength (UTS) is measured from the maximum load supported by the sample, which in turn depends on the onset of necking. The UTS is therefore more dependent on size effects than the yield strength.

Impact testing

The Charpy test itself is recognised to be an empirical measure of toughness, of use in quality control but not as an aid to design. The use of miniature specimens is nevertheless fraught with difficulties because the mechanism of fracture is sensitive to the sample dimensions. The effects of plastic constraint are well documented in standard texts on the subject. There can be no general correlations between measurements on large and small specimens. Miniature specimens should therefore only be used for making comparisons, but with additional caution since brittle fracture may not occur at all.

The critical value K_{IC} of the stress intensity which must be exceeded to induce rapid crack propagation is the product of two terms[90]

$$K_{IC} = \text{stress} \times \text{distance}^{1/2} \qquad (24)$$

where the stress is a fracture stress σ_F which can be measured independently using notched tensile specimens. It can be related to the microstructure via[90–92]

$$\sigma_F \propto \left[\frac{E\gamma_p}{\pi(1-\nu^2)c}\right]^{1/2} \qquad (25)$$

where E is the Young's modulus and ν the Poisson's ratio. γ_p is the effective work done in creating a unit area of crack plane, estimated to be about 14 J m^{-2} for many iron base microstructures; it is much larger than a surface energy (typically 1 J m^{-2}) because of the plastic zone which moves with the crack tip. This value of 14 J m^{-2} seems to apply to a wide variety of steel microstructures, which is surprising given that they often have quite different deformation characteristics. In any event, there is no obvious way of relating γ_p to details of the microstructure. By contrast, the dimension c is usually attributed to the size of a sharp crack created by the fracture of a brittle microstructural constituent such as a cementite particle in wrought steels, or a non-metallic inclusion in a weld deposit.

Lucas and co-workers have found that cleavage fracture stress measured from miniature instrumented impact tests is in excellent agreement with similar measurements from full sized samples (Fig. 29). Notice that the fracture stress is not a complete description of fracture toughness. The other parameter in equation (24), distance$^{1/2}$, refers to a distance ahead of the crack tip, within which the stress is large enough to cause the fracture of brittle crack initiators. The latter are unlikely to be distributed homogeneously in the microstructure and so the critical distance may not be identical for small and large samples.

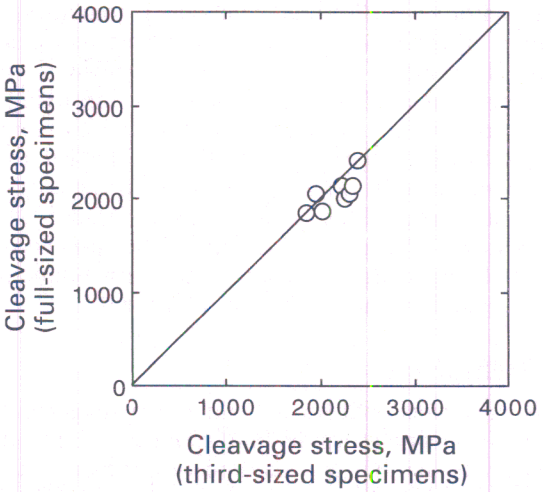

29 Cleavage fracture stress determined from instrumented Charpy specimens; plot compares results from full and one-third sized samples (after Ref. 93)

Regenerative heat treatments

Cavitation and other similar irreversible creep damage does not occur until a late stage in the service life of the creep resistant steels described above. During that period, any loss in properties is due largely to microstructural changes such as carbide coarsening, changes in the configuration of any dislocations, and in the general approach of the microstructure towards equilibrium. Some of these changes can in principle be reversed by regenerating the original microstructure by heating the component back into the austenite phase field, a process which is not often desirable due to the high temperatures involved.

A possible alternative is to regenerate just the carbides, by annealing the steel at a temperature above the service temperature ($\sim$700°C), but below that at which austenite can form.[94] The aim of such a heat treatment would be to dissolve some of the carbides, and reprecipitate them by aging at a lower temperature, thereby regenerating a fine carbide dispersion. The work reported by Senior[94] on a 1Cr–Mo–V steel indicates, however, that 700°C is not high enough to allow a substantial amount of carbide to dissolve, the annealing in fact leading to a further deterioration in the microstructure by accelerating its approach towards equilibrium. For example, in the 1Cr–Mo–V steel, the beneficial V_4C_3 carbide increases in volume fraction but also coarsens rapidly.

Embrittlement may also occur as a consequence of the segregation of impurities to the prior austenite grain surfaces during the course of service at elevated temperatures. The rate of segregation is slow at low temperatures and reduced at high temperatures because entropy effects then become dominant. There is, therefore, an intermediate temperature at which impurity embrittlement is most prominent. Thus,

Yamashita *et al.*[95] found the worst toughness for regions of a Cr–Mo–Ni–V rotor (which had experienced 16 years of service) to occur in regions which had experienced 714 K, the toughness improving for lower and higher temperatures. A heat treatment of the embrittled regions at 811 K for 24 h led to an improvement of toughness even though the hardness did not change. This is presumably because of the evaporation of segregated impurities but also because the carbides at the prior austenite grain boundaries were refined by the 811 K heat treatment.

Conclusions

It is now well understood that the management of aging turbine plant is not simply a means of extending the service life, but is a method of optimising assets without compromising productivity and safety.[96] A large number of methods available for the assessment of remaining life have been reviewed in this paper. These methods can, to varying degrees, be used in combination with experience to design an integrated approach towards life assessment and monitoring.

Acknowledgements

This paper is published with the permission of National Power and Alstom Energy, which make no warranty or representation whatsoever that the information is accurate or can be used for any particular purpose. Any person intending to use the information should satisfy himself of the accuracy thereof and the suitability for the purpose for which he intends to use it. The authors are also grateful to the EPSRC for financial support, to Dr R. Thomson, Dr J. Robson, Mr M. Lord, and Mr N. Fujita for interesting discussions, and to Professor Alan Windle for the provision of laboratory facilities at the University of Cambridge.

References

1. R. W. EVANS and B. WILSHIRE: 'Creep of metals and alloys'; 1985, London, The Institute of Metals.
2. F. B. PICKERING: in 'Microstructural development and stability in high chromium ferritic power plant steels', (ed. A. Strang and D. J. Gooch), 1–29; 1997, London, The Institute of Materials.
3. R. VISWANATHAN: 'Damage mechanisms and life assessment of high-temperature components'; 1989, Metals Park, OH, ASM International.
4. H. K. D. H. BHADESHIA: 'Bainite in steels'; 1992, London, The Institute of Materials.
5. R. D. TOWNSEND: in 'Rupture ductility of creep resistant steels', (ed. A. Strang), 1–16; 1991, London, The Institute of Metals.
6. R. TOWNSEND: in 'Electricity beyond 2000', 251–281; 1991, Palo Alto, CA, Electric Power Research Institute.
7. R. G. CARLTON, D. J. GOOCH, E. M. HAWKES, and H. D. WILLIAMS: in Proc. Conf. 'Refurbishment and life extension of steam plants', 45–52; 1987, London, The Institution of Mechanical Engineering.
8. J. D. PARKER, A. McMINN, and J. FOULDS: in Proc. Conf. 'Life assessment and life extension of power plant components', (ed. T. V. Narayanan), Book no. H00486, 223; 1989, New York, NY, American Society of Mechanical Engineers.
9. D. J. GOOCH and R. D. TOWNSEND: in Proc. EPRI Conf. 'Life assessment and extension of fossil fuel plants', 927–943; 1987, Oxford, Pergamon Press.
10. D. J. GOOCH, M. S. SHAMMAS, M. C. COLEMAN, S. J. BRETT, and R. A. STEVENS: in Proc. Conf. 'Fossil power plant rehabilitation', Cincinnati, OH, 1989, ASM International, Paper 8901–004.
11. R. VISWANATHAN: *Mater. Sci. Eng. A*, 1988, **A103**, 131–139.
12. H. E. EVANS: 'Mechanisms of creep fracture'; 1984, Essex, UK, Elsevier Applied Science Publ.
13. E. L. ROBINSON: *Trans. Am. Soc. Mech. Eng.*, 1952, **74**, 777.
14. B. J. CANE and R. D. TOWNSEND: 'Prediction of remaining life in low alloy steels', Report TPRD/L/2674/N84, Leatherhead, Surrey, 1984.
15. T. GOTO: 'Microstructure and mechanical properties of aging materials', Fossil Power Plants session, ASM Fall Meeting, Chicago, IL, 1992, unpublished.
16. D. J. GOOCH, A. STRANG, and S. M. BEECH: in Proc. 5th Int. Conf. on 'Creep and fracture of engineering materials', (ed. B. Wilshire and R. Evans), 743–763; 1993, London, The Institute of Materials.
17. A. STRANG, S. M. BEECH, and D. J. GOOCH: in 'Materials for advanced power engineering', (ed. D. Coutsouradis *et al.*), Part I, 549–560; 1994, Dordrecht, Kluwer Academic Publ.
18. B. W. ROBERTS and A. STRANG: in 'Refurbishment and life extension of steam plant', 205–213; 1987, London, The Institution of Mechanical Engineers.
19. J. MAGUIRE and D. J. GOOCH: in Proc. Int. Conf. 'Life assessment and extension', The Hague, 1988, EPRI (Palo Alto, CA, USA).
20. A. J. TACK, J. M. BREAR, and F. J. SECO: in 'Creep: characterisation, damage and life assessment', (ed. D. A. Woodford *et al.*), 609–616; 1992, Materials Park, OH, ASM International.
21. D. KALISH, S. A. KULIN, and M. COHEN: *J. Met.*, 1965, **17**, (2), 157–164.
22. T. GLADMAN: 'The physical metallurgy of microalloyed steels', 189; 1997, London, The Institute of Materials.
23. R. W. K. HONEYCOMBE and H. K. D. H. BHADESHIA: 'Steel, microstructure and properties', 2nd edn; 1995, London, Edward Arnold.
24. T. HOOGENDORN and M. J. SPANRAFT: in 'Microalloying '75', 75; 1975, Metals Park, OH, ASM International.
25. J. J. JONAS and I. WEISS: *Met. Sci.*, 1979, **13**, 238–245.
26. T. CHANDRA, M. G. AKBEN, and J. J. JONAS: in Proc. 6th Conf. 'Strength of metals and alloys', (ed. R. C. Gifkins), 499; 1982, Oxford, Pergamon Press.
27. K. A. RIDAL and A. G. QUARRELL: *J. Iron Steel Inst.*, 1962, **200**, 366–373.
28. M. C. MURPHY and G. D. BRANCH: *J. Iron Steel Inst.*, 1969, **207**, 1347–1364.
29. D. KALISH and M. COHEN: *Mater. Sci. Eng.*, 1970, **6**, 156–166.
30. H. K. D. H. BHADESHIA: *Acta Metall.*, 1980, **28**, 1103–1114.
31. B. J. CANE and J. A. WILLIAMS: *Int. Mater. Rev.*, 1987, **32**, 241–262.
32. M. ASKINS and K. MENZIES: unpublished work, Central Electricity Generating Board, Leatherhead, UK, 1985, referred to in Ref. 9.
33. P. BATTAINI, D. D'ANGELO, G. MARINO, and J. HALD: in 'Creep and fracture of engineering materials and structures', 1039–1054; 1990, London, The Institute of Metals.
34. S. D. MANN, D. G. McCULLOCH, and B. C. MUDDLE: *Metall. Mater. Trans. A*, 1995, **26A**, 509–520.
35. R. B. CARRUTHERS and M. J. COLLINS: 'Microstructural technique for assessment of effective operating temperature', Report NER/SSD/M/80/327, Central Electricity Generating Board, Leatherhead, UK, 1980.
36. R. B. CARRUTHERS and M. J. COLLINS: in 'Quantitative microanalysis with high spatial resolution', 108–111; 1981, London, The Metals Society.
37. R. B. CARRUTHERS and M. J. COLLINS: *Met. Sci.*, 1983, **17**, 107–110.
38. A. AFROUZ, M. J. COLLINS, and R. PILKINGTON: *Met. Technol.*, 1983, **10**, 461–463.
39. H. K. D. H. BHADESHIA: *Mater. Sci. Technol.*, 1989, **5**, 131–137.
40. R. SINGH and S. BANERJEE: *Scr. Metall. Mater.*, 1990, **24**, 1093–1098.
41. S. D. MANN and B. C. MUDDLE: in 'Microstructures and mechanical properties of aging material', (ed. P. K. Liaw *et al.*), 301–308; 1993, Warrendale, PA, The Minerals, Metals and Materials Society.
42. S. D. MANN and B. C. MUDDLE: in 'Microstructures and mechanical properties of aging materials', (ed. P. K. Liaw *et al.*), 309–317; 1993, Warrendale, PA, The Minerals, Metals and Materials Society.
43. S. D. MANN and B. C. MUDDLE: *Micron*, 1994, **25**, 499–503.
44. H. K. D. H. BHADESHIA: in 'Mathematical modelling of weld phenomena 2', (ed. H. Cerjak and H. K. D. H. Bhadeshia), 71–118; 1995, London, The Institute of Materials.
45. J. CHANCE and N. RIDLEY: *Metall. Trans. A*, 1981, **21A**, 1205–1213.
49. D. VENUGOPALAN and J. S. KIRKALDY: in 'Hardenability'